

A MID-INFRARED IMAGING SURVEY OF EMBEDDED YOUNG STELLAR OBJECTS IN THE ρ OPHIUCHI CLOUD CORE

MARY BARSONY^{1,2,3}

Department of Physics and Astronomy, San Francisco State University, 1600 Holloway Drive,
San Francisco, CA 94132; mbarsony@stars.sfsu.edu

MICHAEL E. RESSLER^{2,3}

Jet Propulsion Laboratory, California Institute of Technology, Mail Stop 169-327, 4800 Oak Grove Drive,
Pasadena, CA 91109; michael.e.ressler@jpl.nasa.gov

AND

KENNETH A. MARSH

Jet Propulsion Laboratory, California Institute of Technology, Mail Stop 168-414, 4800 Oak Grove Drive,
Pasadena, CA 91109; kenneth.a.marsh@jpl.nasa.gov

Received 2004 September 27; accepted 2005 April 18

ABSTRACT

Results of a comprehensive, new, ground-based mid-infrared imaging survey of the young stellar population of the ρ Ophiuchi cloud are presented. Data were acquired at the Palomar 5 m and at the Keck 10 m telescopes with the MIRLIN and LWS instruments, at $0''.5$ and $0''.25$ resolutions, respectively. Of 172 survey objects, 85 were detected. Among the 22 multiple systems observed, 15 were resolved and their individual component fluxes determined. A plot of the frequency distribution of the detected objects with SED spectral slope shows that YSOs spend $\sim 4 \times 10^5$ yr in the flat-spectrum phase, clearing out their remnant infall envelopes. Mid-infrared variability is found among a significant fraction of the surveyed objects and is found to occur for all SED classes with optically thick disks. Large-amplitude near-infrared variability, also found for all SED classes with optically thick disks, seems to occur with somewhat higher frequency at the earlier evolutionary stages. Although a general trend of mid-infrared excess and near-infrared veiling exists progressing through SED classes, with Class I objects generally exhibiting $r_K \geq 1$, flat-spectrum objects with $r_K \geq 0.58$, and Class III objects with $r_K = 0$, Class II objects exhibit the widest range of r_K values, ranging from $0 \leq r_K \leq 4.5$. However, the highly variable value of veiling that a single source can exhibit in any of the SED classes in which active disk accretion can take place is striking and is direct observational evidence for highly time-variable accretion activity in disks. Finally, by comparing mid-infrared versus near-infrared excesses in a subsample with well-determined effective temperatures and extinction values, disk-clearing mechanisms are explored. The results are consistent with disk clearing proceeding from the inside out.

Subject headings: infrared: stars — ISM: individual (ρ Ophiuchi Cloud) —
planetary systems: protoplanetary disks — stars: formation —
stars: pre-main-sequence — surveys

Online material: machine-readable tables

1. INTRODUCTION

The ρ Ophiuchi cloud core continues to be the subject of intense study at all wavelengths, since it harbors the nearest site of the formation of several hundred young stellar objects (YSOs). Mid-infrared (MIR) observations of ~ 2 dozen YSOs in the ρ Oph cloud core resulted in the development of the currently accepted classification scheme for such objects (Lada & Wilking 1984; Lada 1987). The most comprehensive previous ground-based MIR survey of the ρ Oph clouds included 56 objects, 49 of which were in the central L1688 cloud core (Greene et al. 1994). A

survey of the entire YSO population of the ρ Oph cloud core became practicable for the first time with the advent of MIR arrays mounted on large-aperture ground-based telescopes toward the end of the last decade. It is just such a survey that is the subject of this work.

MIR studies of YSOs are especially relevant for studies of young, planet-forming disks, since MIR emission peaks at distances of order ~ 1 AU from the central object. By contrast, near-infrared (NIR) continuum emission from hot dust originates closer to the central YSO (Eisner et al. 2003; Millan-Gabet et al. 1999, 2001). Comparison of the NIR and MIR properties of young disks is useful for understanding disk structures (Chiang & Goldreich 1997), whereas multiepoch comparison of MIR fluxes with previous (Bontemps et al. 2001) and future (*Spitzer* Legacy and GTO) observations will aid our understanding of disk accretion processes.

Of obvious importance for planet formation are not only studies of average YSO disk lifetimes (e.g., Haisch et al. 2001) but also studies of disk dissipation processes (Armitage et al. 2003). Comparative studies of the population of very young

¹ Space Science Institute, 4750 Walnut Street, Suite 205, Boulder, CO 80301.

² Visiting Astronomer at the W. M. Keck Observatory, which is operated as a scientific partnership among the California Institute of Technology, the University of California, and the National Aeronautics and Space Administration. The Observatory was made possible by the generous financial support of the W. M. Keck Foundation.

³ Observations with the Palomar 5 m telescope were obtained under a collaborative agreement between Palomar Observatory and the Jet Propulsion Laboratory.

(≤ 1 Myr), diskless YSOs (Wilking et al. 2001) with the equally young population of YSOs with optically thick disks detected in the present survey should greatly aid our understanding of the reason for the observed widely varying disk dissipation timescales.

Finally, no current space-based observatory can match the angular resolution achievable from the ground at MIR wavelengths, which is ideal for studying young binaries and their disks at the distance to the ρ Oph clouds. Since the majority of young stars form in binary/multiple systems, studies of planet-forming disks must, of necessity, include studies of the disks in multiple systems. The binary separation of YSOs at the distance to the ρ Oph clouds peaks near a projected angular separation of $0''.25$ (Barsony et al. 2003), which is the diffraction limit of the Keck 10 m telescopes at $10 \mu\text{m}$.

In the following we describe the source selection criteria for our MIR survey, along with the data acquisition and data reduction procedures in § 2. The key results of our new, MIR survey are presented in § 3, and the implications of these are discussed in § 4.

2. SOURCE SELECTION CRITERIA, OBSERVATIONS, AND DATA REDUCTION

The starting point for our target list was the NIR imaging survey (Barsony et al. 1997; hereafter BKLT survey) of the central square degree of the ρ Ophiuchi cloud core (also known as L1688), which catalogs 4495 objects. To winnow this source list to a manageable number of target objects, while maximizing the likelihoods of cloud membership and of MIR detectability, we imposed combined NIR brightness and color criteria. Target objects for this study were, therefore, required to be bright at $2.2 \mu\text{m}$ ($K \leq 13.0$), since YSOs are generally bright NIR emitters, even when highly reddened, and had to have very red NIR color ($H - K \geq 1.67$), since high NIR excess is generally a disk indicator.

Since ρ Oph is, for the most part, a low-mass star-forming cloud, at its distance of 140 pc, the apparent magnitude range $5 \leq K \leq 10.5$ essentially encompasses its entire population, not allowing for extinction. According to theoretical pre-main-sequence (PMS) isochrones, 1 million year old YSOs at the hydrogen-burning limit of $\approx 0.08 M_{\odot}$ should have an apparent $K = 10.5$ at this distance, with no foreground extinction (Wilking et al. 1999). At the other end of the mass spectrum, a similarly youthful Herbig Ae star of $4 M_{\odot}$, WL 16, is observed to have an apparent $K = 7.92$ in ρ Oph, seen through $A_V = 31$ (Ressler & Barsony 2003).

Using the relation $A_K = 1.4(H - K)$, our color selection criterion of $H - K \geq 1.67$ would result in $A_K \geq 2.3$, assuming an intrinsic $(H - K)_0 = 0.0$ (Cohen et al. 1981). Using the relation $A_V = 15.4[(H - K)_{\text{obs}} - (H - K)_0]$ and noting that $(H - K)_0 = 0.3$ for an M dwarf with no infrared excess, our color selection criterion of $H - K \geq 1.67$, when combined with our apparent brightness criterion of $K \leq 13$, guarantees that we are sampling the cloud core's embedded population through $A_V \sim 21$ even for young brown dwarfs. At the other end of the brightness scale, these selection criteria could also include occasional stray background K and M giants out to ~ 1 kpc, depending on the actual obscuration along the line of sight. In fact, the most recent NIR spectroscopic survey of the ρ Ophiuchi YSO population has shown that of the 80 objects in common to both surveys, only 6 of our target list (Elias 35, GY 232, VSSG 6, GY 65, GY 45, BKLT J162618–242818) are confirmed background K or M giants (Luhman & Rieke 1999).

The combined color and brightness criteria described above, when applied to the BKLT survey, selected 104 of 4495 objects,

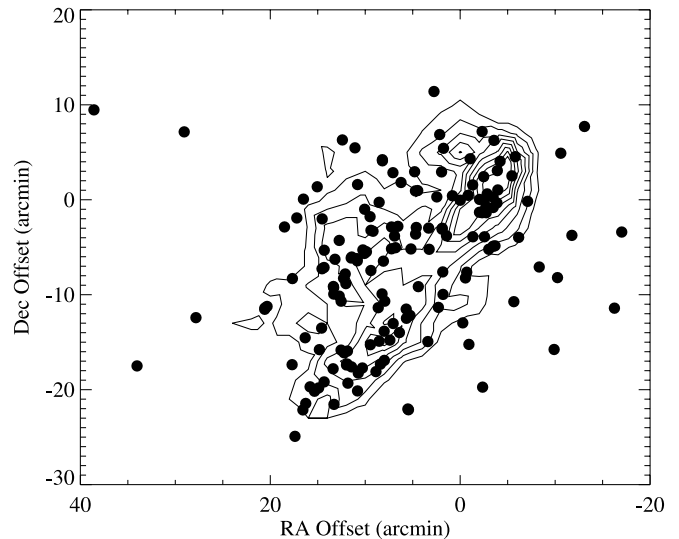


FIG. 1.—Spatial distribution of the target objects for which MIR fluxes and/or flux upper limits are listed in Table 2. The contour plot (courtesy of B. A. Wilking) shows the $\text{C}^{18}\text{O } J = (2 \rightarrow 1)$ integrated intensity in K km s^{-1} units, at 1 K km s^{-1} intervals, starting at 3 K km s^{-1} and ending at 11 K km s^{-1} . The offsets (in arcmin units) are from the (0, 0) position of S1: $\alpha_{\text{J2000.0}} = 16^{\text{h}}26^{\text{m}}34^{\text{s}}.2$, $\delta_{\text{J2000.0}} = -24^{\circ}23'27''$.

of which all but 7 (GY 12, GY 30, IRS 26, BKLT 162805–243354, GY 312, BKLT 162629–241748, and BKLT 162735–244628) were observed by us in the MIR. This source list was supplemented with objects that were known or suspected to be cloud members from various optical emission line, NIR, and far-infrared (FIR) surveys, but which did not satisfy the above-mentioned combined color and brightness criteria (Struve & Rudkjøbing 1949; Dolidze & Arakelyan 1959; Vrba et al. 1975; Elias 1978; Wilking & Lada 1983; Young et al. 1986; Wilking et al. 1989; Leous et al. 1991; Greene & Young 1992; Barsony et al. 1997; Comeron et al. 1993). In total, we report MIR fluxes or flux upper limits for 172 individual objects. The spatial distribution of the objects targeted by this survey is plotted in Figure 1, overlaid on the contours of $\text{C}^{18}\text{O } (J = 2 \rightarrow 1)$ emission from the cloud core, for reference (Wilking & Lada 1983).

The MIR imaging data for this survey of the ρ Oph cloud core's embedded population were obtained with MIRLIN, JPL's 128×128 pixel Si:As camera (Ressler et al. 1994), and the University of California's Long Wavelength Spectrometer (LWS; Jones & Puetter 1993). The relevant observing and data reduction parameters are listed in Table 1. The first column lists the UT date of observation, while the second column specifies the telescope used. All observations at Palomar and on Keck II were made with MIRLIN, whereas LWS was the instrument used on Keck I.

The MIRLIN data were acquired at N band ($\lambda_0 = 10.78 \mu\text{m}$, $\Delta\lambda = 5.7 \mu\text{m}$). However, in order to avoid saturating the medium well depth Si:As detector of the LWS instrument, a narrower band, $12.5 \mu\text{m}$ filter ($\lambda_0 = 12.5 \mu\text{m}$, $\Delta\lambda = 1.0 \mu\text{m}$) was used. MIRLIN has a plate scale of $0''.138 \text{ pixel}^{-1}$ and a $17''.7 \times 17''.7$ field of view at the Keck II telescope; corresponding values for MIRLIN at the Palomar 5 m are $0''.15 \text{ pixel}^{-1}$ and $19''.2 \times 19''.2$, respectively. At the Keck I telescope, the LWS instrument has a plate scale of $0''.08 \text{ pixel}^{-1}$ and a $10''.2 \times 10''.2$ field of view. For reference, the FWHM of a diffraction-limited image at N band is $\sim 0''.25$ at the Keck Telescopes and $0''.47$ at the Palomar 5 m.

TABLE 1
OBSERVING LOGS AND DATA REDUCTION PARAMETERS

UT Date of Observation	Telescope	Observed Standards	Standard-Star N (mag)	Standard-Star Aperture Radius (arcsec)	Target Object Aperture Radius (arcsec)	Aperture Correction	Air-Mass Correction (mag per air mass)	Zero Point
1996 Apr 24.....	P200"			2.1	1.2	1.13 \pm 0.046	0.09	13.65
		α Boo	-3.19					
1997 Jun 26	P200"	α Sco	-4.54	2.1	1.2	1.298 \pm 0.104	0.29	13.71
		σ Sco	+2.40					
		α Lyr	+0.00					
		α Sco	-4.54					
1997 Jun 27	P200"	μ Cep	-3.84	2.1	1.2	1.268 \pm 0.0388	0.25 \pm 0.05	13.74
		σ Sco	+2.40					
		α Lyr	+0.00					
1998 Jun 7	Keck II	α Cr B	+2.19	2.1	0.69	1.134 \pm 0.0227	0.00 \pm 0.06	15.35 \pm 0.04
		γ Aql	-0.78					
1998 Jun 30	P200"	ϕ Oph	+2.20	2.1	1.2	1.136 \pm 0.029	0.30 \pm 0.05	13.94
		WL 12	+3.78					
1998 Jul 1	P200"	μ Cep	-3.84	2.1	1.2	1.105 \pm 0.018	0.26 \pm 0.03	13.87
		γ Aql	-0.78					
		ϕ Oph	+2.20					
1999 Jun 28	LWS/Keck I	α Boo	-3.19	2.0	0.72	1.142 \pm 0.015	-0.03	13.61
		σ Sco	+2.40					
1999 Jun 29	LWS/Keck I	μ UMa	-1.03	2.0	0.72	1.138 \pm 0.058	0.00	13.71 \pm 0.02
		σ Sco	+2.40					

Data were acquired with traditional MIR chopping and nodding techniques. Specifically, for MIRLIN observations, the telescope's secondary mirror was chopped 8" in a north-south direction, at a rate of a few hertz; then the entire telescope was nodded 8" east-west, in order to remove residual differences in the background level. Total on-source integration times were typically 24–25 s at each telescope for the program sources. On-source integration times consisted of several hundred to a thousand co-added chop pairs, with 5–6 ms integration times per frame. For the LWS observations, the secondary mirror chop throw was 4", as was the telescope nod, 4" alternately on either side of the source along a straight line. The LWS chop frequency was 4.8 Hz, integration times per frame were 15 ms, and typical total on-source integration times were 72 s. All raw images were background subtracted, shifted, and co-added with our in-house IDL routine, "mac" (match-and-combine).

The flux standards observed for each night are listed in the third column of Table 1, along with corresponding N -band magnitudes in the fourth column. These were also used for air-mass monitoring. Photometry for the standard stars was performed in circular software apertures with radii (in arcsecond units) indicated in the fifth column of Table 1. A straight line fit to the instrumental minus true magnitudes of the standards as a function of air mass for each night resulted in the determination of the air-mass corrections and zero-point offsets listed in the eighth and ninth columns of Table 1, respectively. No air-mass corrections were used for the Keck data, whereas typical air-mass corrections at Palomar were of order 0.1–0.2 mag per air mass. Photometric consistency between all standards during a given night's observing was typically of order ± 0.05 mag. By adding the errors in the zero-point offsets, the air-mass cor-

rections, the aperture corrections, and the uncertainties in the magnitudes of the standards in quadrature and taking the square root, we estimate the total photometric accuracy of the Keck data to be good to ± 0.06 mag, and the Palomar data to ± 0.08 mag. To convert these errors to janskys, note that 0.00 mag at N band with MIRLIN corresponds to 33.4 Jy, whereas 0.00 mag at 12.5 μ m with LWS corresponds to 25.2 Jy.

Photometry for program sources was typically performed in the software apertures listed in the sixth column of Table 1, under the column heading "Target Object Aperture Radius." Aperture corrections were derived from the flux standards for each night and applied to each target object's instrumental magnitude before application of the zero-point calibration and air-mass correction. The aperture corrections for each night's observing are listed in the seventh column of Table 1. For bright sources with $N \leq 3.5$, the same software apertures were used as for the bright standards. For the case of sources so extended that they appear significantly brighter in a larger software aperture, a software aperture large enough to include all of the detected flux was used.

In the case of close companions, the combined system flux was first determined from a software aperture chosen to be large enough to contain both objects. Subsequently, the relative photometry of each component was determined by fitting a known point-source calibrator (generally one of the flux calibrators observed that night) to the individual source peaks. The total flux was then divided among the components in the ratio determined by the relative point-source fitting photometry.

Upper limits were calculated in the same apertures as faint target objects. The resultant background-subtracted counts per second were multiplied by a factor of 3 and the result converted

to jansky units. Averaging the upper limits obtained in this manner for each telescope/instrument combination, it is found that the mean 1σ flux errors were 0.018 ± 0.024 Jy at $12.5\ \mu\text{m}$ with LWS at Keck I, 0.008 ± 0.005 Jy at $10.8\ \mu\text{m}$ with MIRLIN at Keck II, and 0.029 ± 0.033 Jy at $10.8\ \mu\text{m}$ with MIRLIN at Palomar.

3. RESULTS

The MIR photometry for our target objects is presented in Table 2. The list is right ascension ordered. The first column of Table 2 lists the BKL source name, and the third and fourth columns list the objects' J2000.0 coordinates from Barsony et al. (1997). For reference, the second column of Table 2 lists a common, alternative alias for each BKL object (for cross-references of aliases for infrared sources see Barsony et al. 1997). The fifth and sixth columns list each object's MIR flux or flux upper limit in jansky units (either at $10.8\ \mu\text{m}$ for MIRLIN data or at $12.5\ \mu\text{m}$ for LWS data). The seventh column lists the UT date of observation, and the eighth column lists the telescope/instrument combination used. In some cases, several entries exist for the same object, if it was observed on more than one occasion. In such instances, the different measurements are separately tabulated.

In Figures 2 and 3 we compare our results with ISOCAM photometry (Bontemps et al. 2001). These authors list photometry for 212 objects, of which 199 are in the L1688 cloud core and the rest are in L1689. There are 120 members of L1688 common to both surveys. Figure 2 is a plot of detected objects from Table 2 that are in common with ISOCAM-detected objects. Figure 3 is a plot of sources with upper limits listed in Table 2 that are in common with ISOCAM-detected objects.

In Figure 2 we compare our ground-based MIR photometry for 69 sources that were detected in both ISOCAM filters. The published ISOCAM fluxes are for filters centered at 6.7 and $14.3\ \mu\text{m}$. For comparison with MIRLIN data, whose broadband N filter is centered at $10.8\ \mu\text{m}$, we linearly interpolated the published ISOCAM fluxes to $10.8\ \mu\text{m}$. These objects are represented by filled diamonds in Figure 2. For comparison with LWS data, whose narrower filter was centered at $12.5\ \mu\text{m}$, we linearly interpolated the published ISOCAM fluxes to $12.5\ \mu\text{m}$. These objects are represented by filled squares in Figure 2. The straight line plotted in Figure 2 represents perfect agreement between the measurements reported in this survey and the interpolated measurements from ISOCAM. The agreement is generally good between the two data sets. This means that the ground-based fluxes agree with the ISOCAM fluxes to within 3σ of the published uncertainties. For the sources with good agreement between the ground-based and ISOCAM fluxes, we can infer that any extended emission on scales $\leq 18''$ is below our detection limit, since $18''$ diameter apertures were used for the ISOCAM flux measurements (except for the faintest sources, for which a $9''$ diameter aperture was used), whereas a much smaller software aperture was used for the ground-based flux measurements (see Table 1). Sources whose measured fluxes have larger discrepancies between the ground-based and ISOCAM values are either intrinsically variable or have significant extended emission. These are listed in Table 3 and discussed in § 4.2.

Four objects in common to both surveys, BKL J162609–243411 (SR-3), BKL J162634–242330 (S1), BKL J162702–243726 (WL 16), and BKL J162659–243458 (WL 22), do not have ISOCAM fluxes available, although they are strong MIR emitters. All four are inferred to be embedded early-type stars associated with extended MIR emission (Bontemps et al. 2001). For SR-3, a star of spectral type A0 (Struve & Rudkjøbing 1949), we find a $10.8\ \mu\text{m}$ flux of 0.15 Jy (see Table 2), whereas

its previously published N -band flux, observed through a $6''$ or $8''$ aperture, was 0.36 Jy (Lada & Wilking 1984). These findings are consistent with the presence of extended MIR emission for this source. For S1, a star of B4 spectral type (Bouvier & Appenzeller 1992), we find a $10.8\ \mu\text{m}$ flux of 0.065 Jy, corresponding to $N = 6.77$ (see Table 2). Previous ground-based MIR photometry for this object was 4.9 mag at $11.1\ \mu\text{m}$ in an unspecified, but presumably larger, aperture (Vrba et al. 1975), consistent with the presence of extended MIR emission centered on S1. This object is listed as displaying a double-peaked spectral energy distribution (SED) by Wilking et al. (2001). A detailed, spatially resolved study of the embedded Herbig Ae star, WL 16, shows that the extended MIR emission from this source originates from a ~ 900 AU diameter inclined disk composed of polycyclic aromatic hydrocarbon (PAH) and very small grain (VSG) particles, obscured by a foreground extinction of $A_V = 31$ mag (Ressler & Barsony 2003). WL 22 is inferred to be of early spectral type due to its relatively high infrared luminosity, strong, extended, MIR emission, and lack of millimeter continuum flux.

Figure 3 is a plot of the objects common to both surveys, for which only upper limits are available from the ground-based observations reported here. Filled diamonds indicate $10.8\ \mu\text{m}$ flux upper limits derived from MIRLIN observations; filled squares indicate $12.5\ \mu\text{m}$ flux upper limits derived from LWS observations. Downward-pointing arrows represent the ISOCAM upper limits. Again, the published ISOCAM fluxes are for filters centered at 6.7 and $14.3\ \mu\text{m}$. For cases where both 6.7 and $14.3\ \mu\text{m}$ ISOCAM fluxes are available, we have linearly interpolated the ISOCAM fluxes to $10.8\ \mu\text{m}$ for direct comparison with the MIRLIN data (*filled diamonds*) and to $12.5\ \mu\text{m}$ for direct comparison with the LWS data (*filled squares*). For those cases where only $6.7\ \mu\text{m}$ ISOCAM fluxes were available, we have taken the quoted 15 mJy completeness limit at $14.3\ \mu\text{m}$ as if it were the actually measured $14.3\ \mu\text{m}$ flux, to derive strict interpolated ISOCAM upper limits at 10.8 and $12.5\ \mu\text{m}$ for comparison with the ground-based upper limits.

In Figure 3, the straight line is a locus of points representing perfect agreement between ground-based photometry and the interpolated ISOCAM fluxes. Only one object, GY 301, has an inferred $10.8\ \mu\text{m}$ ISOCAM flux that differs significantly from the ground-based measurement at this wavelength.

There remain 78 members of the L1688 cloud core for which only ISOCAM photometry is available. Of these, only 3 met this survey's primary selection criteria of $K \leq 13.0$ and $H - K \geq 1.67$. These three objects (GY 12, IRS 26, and GY 312) are a subset of the 7 objects listed in § 2 that met our selection criteria but were unobserved by us. Conversely, there are 4 sources meeting our selection criteria and not observed by us, which fell within the areas of L1688 surveyed by ISOCAM, but which are not listed among the 199 L1688 cloud members. These objects are GY 30, BKL 162629–241748, BKL 162735–244628, and BKL 162805–243354. It is likely that the first 3 of these have MIR colors of background objects and were excluded from membership in the L1688 cloud on that basis. Note, however, that GY 30 has recently been discovered to drive a molecular outflow and illuminates a fan-shaped reflection nebulosity (Kamazaki et al. 2003; Dent et al. 1995). The source, BKL 162805–243354, just $4''$ south of GY 472, may not have been resolved with ISOCAM. In summary, all of the objects meeting our selection criteria, but unobserved by us, merit further investigation.

Finally, 41 objects in Table 2, of which 37 fell within the ISOCAM survey's field of view, are not listed among the L1688 cloud members observed by ISOCAM. The fact that only flux

TABLE 2
MID-INFRARED FLUXES FOR ρ OPH SOURCES

BKLT ^a	Aliases	α (J2000.0)	δ (J2000.0)	10.8 μ m Flux ^{b,c} (Jy)	12.5 μ m Flux ^{b,c} (Jy)	Date of Observation	Telescope/Instrument
162522–243452	SR 2	16 25 19.45	–24 26 51.5	≤0.033		1998 Jul 1	P200/MIRLIN
162536–241544	IRS 2	16 25 36.76	–24 15 44.8	0.298		1998 Jul 1	Keck II/MIRLIN
162542–242712	IRS 7	16 25 42.5	–24 27 12.9	≤0.064		1998 Jul 1	P200/MIRLIN
162547–241833	IRS 8	16 25 47.7	–24 18 33.6	≤0.033		1998 Jul 1	P200/MIRLIN
162549–243139	IRS 9	16 25 49.14	–24 31 39.6	≤0.020		1998 Jul 1	P200/MIRLIN
162550–243913	IRS 10	16 25 50.66	–24 39 13.9	≤0.050		1998 Jul 1	P200/MIRLIN
162556–242050	SR 4	16 25 56.17	–24 20 50.5	0.81		1997 Jun 26	P200/MIRLIN
162557–243032	IRS 13=GSS 20	16 25 57.62	–24 30 32.5	≤0.068		1998 Jul 1	P200/MIRLIN
162603–242337	Elias 14=DoAr 21	16 26 03.01	–24 23 37.9	0.206		1998 Jun 30	P200/MIRLIN
162607–242725		16 26 07.15	–24 27 25.6		0.143	1999 Jun 28	Keck I/LWS
162608–241855	CRBR 4	16 26 08.75	–24 18 55.2	≤0.069		1998 Jun 30	P200/MIRLIN
162608–241855	CRBR 4	16 26 08.75	–24 18 55.2	≤0.047		1998 Jun 7	Keck II/MIRLIN
162609–243411	SR 3	16 26 09.35	–24 34 11.1	0.148		1998 Jun 7	Keck II/MIRLIN
162610–242056	GSS 26	16 26 10.28	–24 20 56.6	1.01		1997 Jun 27	P200/MIRLIN
162615–241924	CRBR 9	16 26 15.77	–24 19 24.6		≤0.023	1999 Jun 29	Keck I/LWS
162616–242225	Elias 18=GSS 29	16 26 16.81	–24 22 25.3	0.397		1998 Jul 1	P200/MIRLIN
162616–242225	Elias 18	16 26 16.81	–24 22 25.3	0.372		1998 Jun 30	P200/MIRLIN
162617–242023	Elias 19	16 26 17.02	–24 20 23.9	0.404		1998 Jul 1	P200/MIRLIN
162617–242347	CRBR 12	16 26 17.21	–24 23 47.7	0.315		1997 Jun 27	P200/MIRLIN
162618–242818 ^d		16 26 18.09	–24 28 18.1		1.03	1999 Jun 28	Keck I/LWS
162618–241712		16 26 18.60	–24 17 12.7		≤0.003	1999 Jun 28	Keck I/LWS
162618–242416	CRBR 15	16 26 18.95	–24 24 16.6		0.074	1999 Jun 28	Keck I/LWS
162618–242310	CRBR 17	16 26 18.98	–24 23 10.1	≤0.005		1998 Jun 7	Keck II/MIRLIN
162619–242820	Elias 20=VSSG 1	16 26 19.03	–24 28 21	0.732		1997 Jun 27	P200/MIRLIN
162620–242840		16 26 20.98	–24 28 40.8	≤0.089		1998 Jul 1	P200/MIRLIN
162621–242306	GSS 30 IRS 1	16 26 21.42	–24 23 06.4	8.52		1998 Jun 7	Keck II/MIRLIN
162621–242306	GSS 30 IRS 1	16 26 21.42	–24 23 06.4	8.17		1998 Jun 30	P200/MIRLIN
162621–242306	GSS 30 IRS 3	16 26 21.72	–24 22 50.2	≤0.12		1998 Jun 30	P200/MIRLIN
162622–242449	CRBR 23	16 26 22.16	–24 24 49.9		≤0.019	1999 Jun 28	Keck I/LWS
162622–242409	GY 11	16 26 22.28	–24 24 09.3	≤0.076		1998 Jul 1	P200/MIRLIN
162622–242409	GY 11	16 26 22.28	–24 24 09.3	≤0.020		1998 Jun 30	P200/MIRLIN
162622–242721	GY 14	16 26 22.96	–24 27 21.7		≤0.059	1999 Jun 28	Keck I/LWS
162623–242101	DoAr 24E=Elias 22	16 26 23.34	–24 21 01.8			1998 Jul 1	P200/MIRLIN
	DoAr 24E(primary)			0.625		1998 Jul 1	P200/MIRLIN
	DoAr 24E(secondary) ^c			2.01		1998 Jul 1	P200/MIRLIN
162623–242441	GY 21(secondary)	16 26 23.54	–24 24 41.5	0.398		1998 Jun 30	P200/MIRLIN
162623–242441	GY 21(secondary)	16 26 23.54	–24 24 41.5	0.39		1998 Jul 1	P200/MIRLIN
162623–242603	DoAr 25=GY 17	16 26 23.84	–24 43 11.8	0.26		1998 Jul 1	P200/MIRLIN
162624–242449	Elias 23=GY 23	16 26 24.05	–24 24 49.7			1998 Jul 1	P200/MIRLIN
162624–242449	Elias 23(primary)			2.15		1998 Jul 1	P200/MIRLIN
162624–241616	Elias 24	16 26 24.07	–24 16 16.1	2.57		1997 Jun 26	P200/MIRLIN
162625–242446	GY 29	16 26 25.28	–24 24 46.7	≤0.043		1998 Jun 7	Keck II/MIRLIN
162625–242325	GY 31	16 26 25.24	–24 23 25.7	≤0.021		1998 Jun 7	Keck II/MIRLIN
162628–242153	GY 38	16 26 28.43	–24 21 53.4		≤0.050	1999 Jun 29	Keck I/LWS
162628–242153	GY 38	16 26 28.43	–24 21 53.4	≤0.042		1998 Jun 7	Keck II/MIRLIN
162629–241908	SKS 1–19	16 26 29.6	–24 19 08.0	≤0.079		1997 Jun 27	P200/MIRLIN
162630–243841	GY 45 ^d	16 26 30.16	–24 38 41.1		≤0.070	1999 Jun 29	Keck I/LWS
162630–243841	GY 45 ^d	16 26 30.16	–24 38 41.1		≤0.041	1999 Jun 28	Keck I/LWS
162630–242258	GY 51=VSSG 27	16 26 30.49	–24 22 59			1998 Jun 7	Keck II/MIRLIN
	GY 51(primary)			0.224		1998 Jun 7	Keck II/MIRLIN
	GY 51(secondary)			≤0.018		1998 Jun 7	Keck II/MIRLIN
162631–243105	IRS 14	16 26 31.17	–24 31 05.6	≤0.068		1997 Jun 27	P200/MIRLIN
162631–243141	IRS 15=GY 58	16 26 31.77	–24 31 41.8	≤0.060		1998 Jul 1	P200/MIRLIN
162633–243625	GY 65 ^d	16 26 33.0	–24 36 25.9		≤0.044	1999 Jun 29	Keck I/LWS
162634–242330	Elias 25=S1=GY 70	16 26 34.17	–24 23 30.5	0.065		1998 Jun 7	Keck II/MIRLIN
162637–242302	GY 81	16 26 37.8	–24 23 02.6		0.103	1999 Jun 28	Keck I/LWS
162640–242715	GY 91=CRBR 42	16 26 40.53	–24 27 15.9	0.157		1997 Jun 27	P200/MIRLIN
162641–241801		16 26 41.91	–24 18 02.0		≤0.043	1999 Jun 28	Keck I/LWS
162642–243325	WL 8	16 26 42.15	–24 33 25.5	0.0733		1998 Jun 7	Keck II/MIRLIN
162642–243103	WL 7	16 26 42.28	–24 31 03.3	0.0514		1998 Jun 7	Keck II/MIRLIN
162642–242627	GY 101	16 26 42.50	–24 26 27.4	≤0.021		1997 Jun 27	P200/MIRLIN
162642–242633	GY 103	16 26 42.58	–24 26 33.3	≤0.021		1997 Jun 27	P200/MIRLIN
162642–242633	GY 103	16 26 42.58	–24 26 33.3		≤0.005	1999 Jun 28	Keck I/LWS

TABLE 2—Continued

BKLT ^a	Aliases	α (J2000.0)	δ (J2000.0)	10.8 μm Flux ^{b,c} (Jy)	12.5 μm Flux ^{b,c} (Jy)	Date of Observation	Telescope/Instrument
162642–242031	Elias 26	16 26 42.81	–24 20 31.9	0.41		1998 Jul 1	P200/MIRLIN
	Elias 26(primary)			0.41		1998 Jul 1	P200/MIRLIN
	Elias 26(secondary)			≤ 0.14		1998 Jul 1	P200/MIRLIN
162643–241635	IRS 19=VSSG 11	16 26 43.67	–24 16 35.7	≤ 0.038		1998 Jul 1	P200/MIRLIN
162644–243447	WL 12	16 26 44.3	–24 34 47.5	1.14		1998 Jul 1	P200/MIRLIN
162644–243447	WL 12	16 26 44.3	–24 34 47.5	1.05		1998 Jun 7	Keck II/MIRLIN
162644–243447	WL 12	16 26 44.3	–24 34 47.5		0.888/0.967	1999 Jun 29	Keck I/LWS
162645–242309	Elias 27	16 26 45.01	–24 23 09.6	0.32		1998 Jul 1	P200/MIRLIN
162646–241203	VSS 27	16 26 46.31	–24 12 03.5	0.285		1998 Jul 1	P200/MIRLIN
162646–241203	VSS 27	16 26 46.31	–24 12 03.5		0.296	1999 Jun 28	Keck I/LWS
	WL 2	16 26 48.56	–24 28 40.4	0.184		1996 Apr 24	P200/MIRLIN
	WL 2	16 26 48.56	–24 28 40.4	0.155		1998 Jun 7	Keck II/MIRLIN
162648–242836	WL 2N (secondary)			≤ 0.029		1996 Apr 24	P200/MIRLIN
162648–242836	WL 2N			0.0163		1998 Jun 7	Keck II/MIRLIN
162648–242840	WL 2S (primary)			0.186		1996 Apr 24	P200/MIRLIN
162648–242840	WL 2S			0.139		1998 Jun 7	Keck II/MIRLIN
162648–242626	GY 130	16 26 48.8	–24 26 26.8	≤ 0.023		1998 Jun 7	Keck II/MIRLIN
162649–243823	WL 18	16 26 49.19	–24 38 23.7			1996 Apr 24	P200/MIRLIN
162649–243823	WL 18	16 26 49.19	–24 38 23.7			1998 Jun 7	Keck II/MIRLIN
	WL 18N(secondary)			≤ 0.041		1996 Apr 24	P200/MIRLIN
	WL 18N			≤ 0.015		1998 Jun 7	Keck II/MIRLIN
	WL 18S(primary)			≤ 0.041		1996 Apr 24	P200/MIRLIN
	WL 18S			0.063		1998 Jun 7	Keck II/MIRLIN
162653–243236	GY 146	16 26 53.59	–24 32 36.5	≤ 0.0285		1998 Jun 7	Keck II/MIRLIN
162653–242229	GY 150=VSSG 6 ^d	16 26 53.85	–24 22 29.7	≤ 0.065		1998 Jul 1	P200/MIRLIN
162654–242622	GY 153=VSSG 5	16 26 54.51	–24 26 22.3	≤ 0.078		1997 Jun 27	P200/MIRLIN
162654–242703	GY 154	16 26 54.84	–24 27 04.0		≤ 0.065	1999 Jun 28	Keck I/LWS
162654–242231	GY 156	16 26 54.97	–24 22 31.4	≤ 0.076		1998 Jul 1	P200/MIRLIN
162655–242030	GSS 41=GY 157	16 26 55.27	–24 20 30.3	≤ 0.039		1997 Jun 27	P200/MIRLIN
162656–242838	GY 163	16 26 56.99	–24 28 38.7		≤ 0.030	1999 Jun 28	Keck I/LWS
162657–243538	WL 21	16 26 57.44	–24 35 38.5	≤ 0.026		1996 Apr 24	P200/MIRLIN
162657–243538	WL 21	16 26 57.44	–24 35 38.5	≤ 0.038		1998 Jun 7	Keck II/MIRLIN
162657–243538	WL 21	16 26 57.44	–24 35 38.5		≤ 0.020	1999 Jun 29	Keck I/LWS
162658–244529	SR 24N(secondary)	16 26 58.46	–24 45 29.9	1.40		1997 Jun 26	P200/MIRLIN
162658–244529	SR 24N	16 26 58.46	–24 45 29.9	1.40		1998 Jun 7	Keck II/MIRLIN
162658–244534	SR 24S(primary)	16 26 58.20	–24 45 34.7	2.01		1997 Jun 26	P200/MIRLIN
162658–244534	SR 24S	16 26 58.52	–24 45 34.7	1.655		1998 Jun 7	Keck II/MIRLIN
162659–243556	WL 14	16 26 59.10	–24 35 56.5	≤ 0.037		1996 Apr 24	P200/MIRLIN
162659–243556	WL 14	16 26 59.10	–24 35 56.5		≤ 0.022	1999 Jun 29	Keck I/LWS
162659–243556	WL 14	16 26 59.1	–24 35 56.5	≤ 0.0146		1998 Jun 7	Keck II/MIRLIN
162659–243458	WL 22	16 26 59.21	–24 34 58.2	0.476		1996 Apr 24	P200/MIRLIN
162659–243458	WL 22	16 26 59.21	–24 34 58.2	0.443		1998 Jun 30	P200/MIRLIN
162659–243458	WL 22	16 26 59.21	–24 34 58.2		0.373/0.560	1999 Jun 29	Keck I/LWS
162701–242138	GY 181	16 27 01.56	–24 21 38.3	≤ 0.10		1998 Jul 1	P200/MIRLIN
162702–243726	WL 16 ^f	16 27 02.35	–24 37 26.5	6.83		1996 Apr 24	P200/MIRLIN
162702–243726	WL 16 ^f	16 27 02.35	–24 37 26.5	5.94		1998 Jun 30	P200/MIRLIN
162703–242615	GY 188	16 27 03.03	–24 26 15.8	≤ 0.069		1997 Jun 27	P200/MIRLIN
162704–242830	WL 1	16 27 04.13	–24 28 30.7	0.130		1998 Jun 7	Keck II/MIRLIN
	WL 1N(secondary)			0.050		1998 Jun 7	Keck II/MIRLIN
	WL 1S(primary)			0.080		1998 Jun 7	Keck II/MIRLIN
162704–242716	GY 195	16 27 04.57	–24 27 16.5	0.059		1998 Jun 7	Keck II/MIRLIN
	LFAM 26/GY 197	16 27 05.25	–24 36 29.4	≤ 0.042		1998 Jun 30	P200/MIRLIN
	LFAM 26/GY 197	16 27 05.25	–24 36 29.4	≤ 0.102		1998 Jul 1	P200/MIRLIN
162705–242036	GY 200	16 27 05.28	–24 20 36.2		≤ 0.052	1999 Jun 29	Keck I/LWS
162705–242619	IRS 30=GY 203	16 27 05.97	–24 26 19.3	≤ 0.038		1998 Jun 7	Keck II/MIRLIN
162705–242619	IRS 30	16 27 05.97	–24 26 19.3	≤ 0.117		1998 Jul 1	P200/MIRLIN
162705–242619	IRS 30	16 27 05.97	–24 26 19.3		≤ 0.093	1999 Jun 29	Keck I/LWS
162706–242837	GY 202	16 27 06	–24 28 37.3	≤ 0.04		1998 Jul 1	P200/MIRLIN
162706–243814	WL 17	16 27 06.79	–24 38 14.6		0.825	1999 Jun 29	Keck I/LWS
162709–243408	WL 10	16 27 09.13	–24 34 08.1	0.163		1998 Jun 7	Keck II/MIRLIN
162709–244022	GY 213	16 27 09.35	–24 40 22.5		0.154	1999 Jun 28	Keck I/LWS
162709–243718	WL 15	16 27 09.43	–24 37 18.5	24.2		1998 Jun 7	Keck II/MIRLIN
162709–243718	WL 15	16 27 09.43	–24 37 18.5	23.7		1997 Jun 26	P200/MIRLIN
162709–242955	GY 215	16 27 09.74	–24 29 55.8	≤ 0.015		1998 Jun 7	Keck II/MIRLIN
162709–242955	GY 215	16 27 09.74	–24 29 55.8		≤ 0.087	1999 Jun 29	Keck I/LWS

TABLE 2—Continued

BKLT ^a	Aliases	α (J2000.0)	δ (J2000.0)	10.8 μm Flux ^{b,c} (Jy)	12.5 μm Flux ^{b,c} (Jy)	Date of Observation	Telescope/Instrument
162710–241914	SR 21N(primary)	16 27 10.17	–24 19 14.8	1.73		1997 Jun 26	P200/MIRLIN
162710–241921	SR 21S(secondary)			≤ 0.211		1997 Jun 26	P200/MIRLIN
	SR 21S	16 27 10.14	–24 19 21.2		≤ 0.024	1999 Jun 28	Keck I/LWS
162710–243322	WL 9	16 27 10.39	–24 33 22.6	≤ 0.0435		1998 Jun 7	Keck II/MIRLIN
162710–243322	WL 9	16 27 10.39	–24 33 22.6		≤ 0.023	1999 Jun 29	Keck I/LWS
162711–244046	GY 224	16 27 11.17	–24 40 46.7	0.255		1998 Jun 7	Keck II/MIRLIN
162711–242343	IRS 32=GY 228	16 27 11.68	–24 23 43.5	≤ 0.049		1998 Jul 1	P200/MIRLIN
162711–243832	WL 19	16 27 11.74	–24 38 32.1	0.13		1996 Apr 24	P200/MIRLIN
162711–243832	WL 19	16 27 11.74	–24 38 32.1		0.223	1999 Jun 29	Keck I/LWS
162712–243449	WL 11	16 27 12.16	–24 34 49.3	0.0299		1998 Jun 7	Keck II/MIRLIN
162713–244133	GY 232 ^d	16 27 13.25	–24 41 33.3	0.031		1998 Jun 7	Keck II/MIRLIN
162714–242646	IRS 33=GY 236	16 27 14.53	–24 26 46.9	0.062		1998 Jun 7	Keck II/MIRLIN
162715–242640	IRS 34	16 27 15.48	–24 26 40.6	0.172		1998 Jun 7	Keck II/MIRLIN
	IRS 34N(primary)			0.092		1998 Jun 7	Keck II/MIRLIN
	IRS 34S(secondary)			0.080		1998 Jun 7	Keck II/MIRLIN
162715–243054	CRBR 70=IRS 35	16 27 15.54	–24 30 54.1	≤ 0.033		1997 Jun 27	P200/MIRLIN
162715–243843	WL 20 ^e	16 27 15.83	–24 38 43.6	0.41		1996 Apr 24	P200/MIRLIN
162715–243843	WL 20 ^e	16 27 15.83	–24 38 43.6	0.55		1998 Jul 1	P200/MIRLIN
	WL 20S	16 27 15.72	–24 38 45.6	0.281		1996 Apr 24	P200/MIRLIN
	WL 20S	16 27 15.72	–24 38 45.6	0.350		1998 Jul 1	P200/MIRLIN
	WL 20E	16 27 15.89	–24 38 43.4	0.079		1996 Apr 24	P200/MIRLIN
	WL 20E	16 27 15.89	–24 38 43.4	0.117		1998 Jul 1	P200/MIRLIN
	WL 20W	16 27 15.69	–24 38 43.4	0.0515		1996 Apr 24	P200/MIRLIN
	WL 20W	16 27 15.69	–24 38 43.4	0.082		1998 Jul 1	P200/MIRLIN
162715–242514	IRS 36=GY 241	16 27 15.88	–24 25 14.8	≤ 0.017		1998 Jun 7	Keck II/MIRLIN
162717–242856	GY 244 ^h	16 27 17.60	–24 28 56.6	0.194		1996 Apr 24	P200/MIRLIN
162717–242856	GY 244 ^h	16 27 17.60	–24 28 56.6		0.37	1999 Jun 28	Keck I/LWS
162718–242853	WL 5 ^h	16 27 18.19	–24 28 53.1	≤ 0.033		1996 Apr 24	P200/MIRLIN
162718–242853	WL 5 ^h	16 27 18.19	–24 28 53.1		0.05	1999 Jun 28	Keck I/LWS
162718–243915	GY 245	16 27 18.38	–24 39 15	0.068		1998 Jun 7	Keck II/MIRLIN
162718–242427	GY 248	16 27 18.39	–24 24 27.6		≤ 0.029	1999 Jun 28	Keck I/LWS
162718–242906	WL 4 ^h	16 27 18.50	–24 29 6.1	0.292		1996 Apr 24	P200/MIRLIN
162718–242906	WL 4 ^h	16 27 18.50	–24 29 06.1		0.40	1999 Jun 28	Keck I/LWS
162719–242844	WL 3 ^h	16 27 19.23	–24 28 44.3	0.162		1997 Jun 27	P200/MIRLIN
162719–242844	WL 3 ^h	16 27 19.23	–24 28 44.3		0.132	1999 Jun 28	Keck I/LWS
162719–244139	SR 12	16 27 19.55	–24 41 40	≤ 0.30		1997 Jun 26	P200/MIRLIN
162721–244142	IRS 42	16 27 21.45	–24 41 42.8	2.03		1997 Jun 27	P200/MIRLIN
162721–242151	GY 255	16 27 21.65	–24 21 51.6		≤ 0.062	1999 Jun 29	Keck I/LWS
162721–244335	GY 253	16 27 21.81	–24 43 35.8	≤ 0.011		1998 Jun 7	Keck II/MIRLIN
162721–244335	GY 253	16 27 21.81	–24 43 35.8		≤ 0.066	1999 Jun 29	Keck I/LWS
162721–242953	WL 6	16 27 21.83	–24 29 53.2	1.08		1996 APR 24	P200/MIRLIN
162721–242953	WL 6	16 27 21.83	–24 29 53.2	1.012		1998 Jun 7	Keck II/MIRLIN
162722–242939	GY 256	16 27 22.0	–24 29 39.9	1.03		1998 Jun 7	Keck II/MIRLIN
162722–241759	VSSG 22	16 27 22.82	–24 17 59.3		≤ 0.053	1999 Jun 29	Keck I/LWS
162724–242929	GY 257	16 27 24.23	–24 29 29.6	≤ 0.023		1998 Jun 7	Keck II/MIRLIN
162724–244147	GY 258	16 27 24.38	–24 41 47.4	≤ 0.051		1998 Jul 1	P200/MIRLIN
162724–244103	CRBR 85	16 27 24.58	–24 41 3.6	0.216		1997 Jun 27	P200/MIRLIN
162724–242935	GY 259	16 27 24.66	–24 29 35.4	≤ 0.015		1998 Jun 7	Keck II/MIRLIN
162726–244246	GY 260	16 27 26.27	–24 42 46.4		0.059	1999 Jun 29	Keck I/LWS
162726–243923	GY 262	16 27 26.45	–24 39 23.9	0.177		1998 Jun 7	Keck II/MIRLIN
162726–244045	GY 263	16 27 26.6	–24 40 45.9	0.03		1998 Jun 7	Keck II/MIRLIN
162726–244051	IRS 43=GY 265	16 27 26.9	–24 40 51.5	2.29		1997 Jun 27	P200/MIRLIN
162726–244051	IRS 43=GY 265	16 27 26.9	–24 40 51.5	1.54		1998 Jun 7	Keck II/MIRLIN
162727–243217	GY 266	16 27 27.12	–24 32 17.8	≤ 0.044		1998 Jul 1	P200/MIRLIN
162727–243116	WL 13	16 27 27.43	–24 31 16.9	0.085		1998 Jun 7	Keck II/MIRLIN
162728–243934	IRS 44=YLW 16A	16 27 28.0	–24 39 34.3	2.65		1997 Jun 27	P200/MIRLIN
162728–243143	GY 272	16 27 28.2	–24 31 43.7	≤ 0.030		1998 Jul 1	P200/MIRLIN
162728–242721	Elias 32=IRS 45	16 27 28.44	–24 27 21.9	0.41		1997 Jun 26	P200/MIRLIN
162728–241709		16 27 28.64	–24 17 09.4		≤ 0.005	1999 Jun 28	Keck I/LWS
162729–243408	GY 275	16 27 29.35	–24 34 08.0		≤ 0.029	1999 Jun 28	Keck I/LWS
162729–243917	IRS 46	16 27 29.41	–24 39 17	0.540		1998 Jun 7	Keck II/MIRLIN
162730–242744	Elias 33=GY 279	16 27 30.18	–24 27 44.3	0.954		1997 Jun 27	P200/MIRLIN
162730–243335	GY 278	16 27 30.21	–24 33 36	≤ 0.043		1997 Jun 27	P200/MIRLIN
162732–242943	GY 287	16 27 32.16	–24 29 43.6		≤ 0.037	1999 Jun 28	Keck I/LWS
162732–244500	GY 288	16 27 32.74	–24 45 0.5	≤ 0.007		1998 Jun 7	Keck II/MIRLIN

TABLE 2—Continued

BKLT ^a	Aliases	α (J2000.0)	δ (J2000.0)	10.8 μm Flux ^{b,c} (Jy)	12.5 μm Flux ^{b,c} (Jy)	Date of Observation	Telescope/Instrument
162732–243323	GY 289	16 27 32.75	–24 33 23.5		≤0.039	1999 Jun 28	Keck I/LWS
162732–243242	GY 290	16 27 32.79	–24 32 42.5		≤0.030	1999 Jun 28	Keck I/LWS
162732–243235	GY 291	16 27 32.92	–24 32 35.0		0.087	1999 Jun 28	Keck I/LWS
162733–241115	GY 292=CRBR 90	16 27 33.11	–24 41 15.7		0.551/0.699	1999 Jun 29	Keck I/LWS
162737–242846	GY 303	16 27 37.12	–24 28 46.2	≤0.08		1997 Jun 27	P200/MIRLIN
162737–243035	IRS 48	16 27 37.23	–24 30 35.2	3.91		1998 Jun 30	P200/MIRLIN
162737–243035	IRS 48	16 27 37.23	–24 30 35.2		2.07/2.61	1999 Jun 29	Keck I/LWS
162737–244238	GY 301	16 27 37.28	–24 42 38.7	≤0.047		1997 Jun 27	P200/MIRLIN
162738–242528	GY 309	16 27 38.05	–24 25 28.8	≤0.001		1998 Jun 7	Keck II/MIRLIN
162738–242528	GY 309	16 27 38.05	–24 25 28.8		≤0.035	1999 Jun 29	Keck I/LWS
162738–243043	IRS 50=GY 306	16 27 38.17	–24 30 43.1	≤0.097		1998 Jul 1	P200/MIRLIN
162738–243658	IRS 49	16 27 38.4	–24 36 58.3	0.425		1997 Jun 26	P200/MIRLIN
162739–243914	GY 314	16 27 39.46	–24 39 14.7		0.664	1999 Jun 28	Keck I/LWS
162739–244316	IRS 51	16 27 39.84	–24 43 16.1	1.10		1997 Jun 26	P200/MIRLIN
162740–242205	SR 9	16 27 40.3	–24 22 05.5	0.43		1997 Jun 26	P200/MIRLIN
162741–244337	GY 323	16 27 41.76	–24 43 37.3	0.045		1998 Jun 7	Keck II/MIRLIN
162743–244309	IRS 53=GY 334	16 27 43.81	–24 43 09.4	≤0.064		1998 Jun 7	Keck II/MIRLIN
162743–244309	IRS 53=GY 334	16 27 43.81	–24 43 09.4		≤0.016	1999 Jun 29	Keck I/LWS
162745–244454	GY 344	16 27 45.84	–24 44 54.6		0.117	1999 Jun 28	Keck I/LWS
162746–243759	GY 346	16 27 46.03	–24 37 59.7		≤0.021	1999 Jun 29	Keck I/LWS
162746–242323	Elias 35=GY 351 ^d	16 27 46.70	–24 23 23.8	≤0.052		1998 Jul 1	P200/MIRLIN
162747–244535	GY 352	16 27 47.16	–24 45 35.5		0.052/0.073	1999 Jun 29	Keck I/LWS
162749–242522	GY 371	16 27 49.78	–24 25 22.9	≤0.25		1998 Jul 1	P200/MIRLIN
162750–244822	WLY 54	16 27 50.87	–24 48 22.4	≤0.63		1997 Jun 26	P200/MIRLIN
162751–243145	IRS 54	16 27 51.89	–24 31 45.8	2.51		1997 Jun 26	P200/MIRLIN
162752–244049	IRS 55=GY 380	16 27 52.12	–24 40 49.8	≤0.094		1998 Jul 1	P200/MIRLIN
162752–244049	IRS 55	16 27 52.12	–24 40 49.8	≤0.34		1997 Jun 26	P200/MIRLIN
162755–242619	SR 10=GY 400	16 27 55.49	–24 26 19.0	0.181		1998 Jul 1	P200/MIRLIN
162803–243441	GY 450	16 28 03.66	–24 34 41.6	≤0.060		1998 Jul 1	P200/MIRLIN
162804–243451	GY 461	16 28 04.65	–24 34 51.6	≤0.057		1998 Jul 1	P200/MIRLIN
162804–243459	GY 463	16 28 04.74	–24 34 59.2	≤0.008		1998 Jun 7	Keck II/MIRLIN
162836–243552		16 28 36.61	–24 35 52.8		≤0.40	1999 Jun 29	Keck I/LWS
162841–241618		16 28 41.73	–24 16 18.5	≤0.007		1998 Jun 7	Keck II/MIRLIN
162841–241618		16 28 41.73	–24 16 18.5		≤0.023	1999 Jun 29	Keck I/LWS
162904–244057		16 29 04.01	–24 40 57.3		≤0.060	1999 Jun 28	Keck I/LWS
162923–241359	WLY 64=IRAS 64a	16 29 23.39	–24 13 59.2	0.63		1997 Jun 26	P200/MIRLIN
162923–241359	WLY 64	16 29 23.39	–24 13 59.2	0.478		1998 Jul 1	P200/MIRLIN

NOTES.—Units of right ascension are hours, minutes, and seconds, and units of declination are degrees, arcminutes, and arcseconds. Table 2 is also available in machine-readable form in the electronic edition of the *Astrophysical Journal*.

^a Source designations from Barsony et al. (1997).

^b Upper limits are 3σ .

^c Where two values of 12.5 μm flux are listed, separated by a slash, the first flux is measured in a circular aperture of radius $0''.72$, the second in a circular aperture of radius $2''.0$. Such objects are likely extended in the MIR at these angular scales.

^d Spectroscopically determined background giant (Luhman & Rieke 1999).

^e The secondary in the DoAr 24E system is an infrared companion discovered by Chelli et al. (1988).

^f WL 16 and its extended PAH and VSG disk are thoroughly discussed in Ressler & Barsony (2003); the aperture photometry presented here was measured in $r = 4''$ and $3''.75$ circular apertures, for the data of 1996 April 24 and 1998 June 30, respectively.

^g The combined flux of the WL 20 triple system is listed here. See Ressler & Barsony (2001) for a thorough discussion of this system. Individual source positions for each component are from Barsony et al. (2002).

^h Our chop/nod directions and separations were poorly placed with respect to the WL 3, WL 4, WL 5, and GY 244 asterism. Hence, we quote an upper limit for WL 5 derived from the average values for undetected sources for 1996 April 24, instead of measuring an upper limit directly from the co-added data for this source.

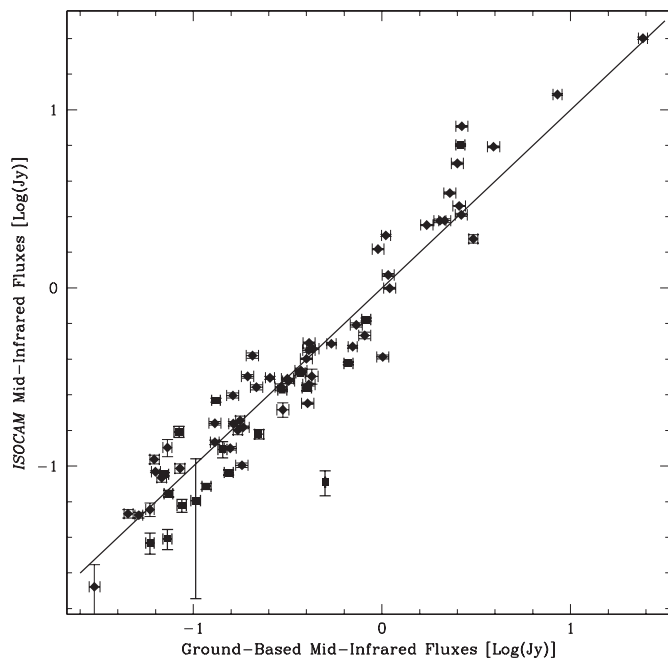


FIG. 2.—Plot of ground-based MIR fluxes for objects in Table 2 vs. MIR fluxes from ISOCAM. The 69 objects plotted here were common to, and detected by, both surveys. Furthermore, each object plotted here was detected through both ISOCAM filters, centered at 6.7 and 14.3 μm , respectively. Filled diamonds represent objects detected by MIRLIN at 10.8 μm , with linearly interpolated ISOCAM 10.8 μm fluxes. Filled squares represent objects detected by LWS at 12.5 μm , with linearly interpolated ISOCAM 12.5 μm fluxes.

upper limits were measured from the ground-based observations reported here for 34 of 37 of these objects is consistent with their being background sources. The three exceptions are GY 263, GY 232, and BKLT 162618–242818, for which there are ground-based detections (see Table 2), but no ISOCAM fluxes are published. Two of these, GY 232 and BKLT 162618–242818, have been spectroscopically determined to be background giants (Luhman & Rieke 1999). The nature of GY 263 remains to be determined. There are 4 objects in this ground-based survey that fell outside of the ISOCAM survey’s field of view: WLY 64=IRAS 64a, SR-2, BKLT 162904–244057, and BKLT 162522–243452. WLY 64 exhibits an M8–M9 III optical spectral type, but a K4 III NIR CO band absorption, very similar to FU Ori objects (Luhman & Rieke 1999). SR-2 has a G8 spectral type and had been assumed to be a foreground object based on its NIR colors (Elias 1978). More recent, high-dispersion, optical spectroscopy has shown SR-2 to be a PMS member of the ρ Oph cloud core, however (Walter et al. 1994). The nature of the other two objects remains to be determined.

4. DISCUSSION

4.1. Relative Timescales within SED Classes: The Flat-Spectrum Objects

For nearly two decades now, young stellar objects have been age ordered according to an empirical classification scheme based on the slope, a , of their NIR (2.2 μm) to MIR (10 μm) SEDs:

$$a = \frac{d \log(\lambda F_\lambda)}{d \log \lambda}.$$

In this scheme, Class I SEDs have $a \geq 0.3$, flat-spectrum SEDs have $-0.3 \leq a \leq +0.3$, Class II SEDs have $-0.3 \geq a \geq -1.6$, and Class III SEDs have $a \leq -1.6$ (Greene et al. 1994). The

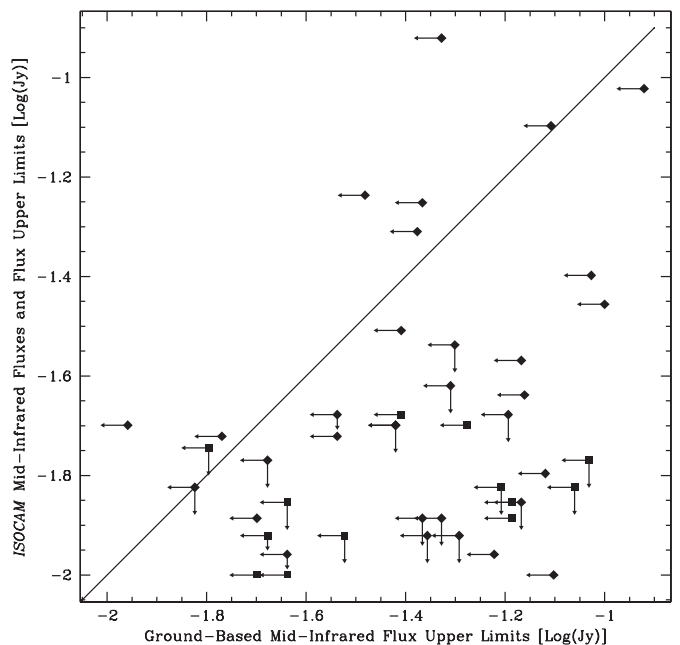


FIG. 3.—Plot of ground-based MIR flux upper limits for objects in Table 2 in common with ISOCAM-detected objects. Filled diamonds represent MIRLIN 10.8 μm upper limits; filled squares represent LWS 12.5 μm upper limits. ISOCAM fluxes were interpolated to 10.8 (filled diamonds) or 12.5 μm (filled squares) for objects detected in both ISOCAM filters. For objects detected only at 6.7 μm by ISOCAM, the 14.3 μm completeness limit of 15 mJy is used to derive the interpolated ISOCAM flux upper limits.

latter authors were the first to suggest that the flat-spectrum SEDs be identified as a distinct class, since YSOs with $+0.3 \geq a \geq -0.3$ were found to have spectra strongly veiled by continuum emission from hot, circumstellar dust, unlike the case for the NIR spectra of typical, classical T Tauri stars (those generally associated with Class II SEDs).

In general, the above spectral slope classes have been found to correspond to distinct physical objects, defined by the amount and geometry of the circumstellar material surrounding the central, forming YSO. Thus, a Class I object is one in which the central YSO has essentially attained its initial main-sequence mass but is still surrounded by a remnant infall envelope and accretion disk; a Class II object is surrounded by an accretion disk; and a Class III object has only a remnant, or absent, accretion disk. The gradual clearing of circumstellar matter has been interpreted as an evolutionary sequence.

In this context, in most cases the SED class reflects the evolutionary state. As a cautionary note, however, there may be instances in which the SED class does not give the correct evolutionary state. For instance, a T Tauri star seen through a great amount of foreground obscuration may display a Class I or flat-spectrum SED (since the 2 μm flux suffers heavier extinction than the 10 μm flux). Additionally, orientation effects can also be very important, since a more pole-on Class I object may have an SED similar to an edge-on Class II object (Whitney et al. 2003). The definitive way to ascertain the evolutionary state of a YSO is to obtain resolved images of the given object at several different infrared wavelengths and to compare these images quantitatively with model images produced using three-dimensional radiative transfer codes (Whitney et al. 2003). Since such data are unavailable for our current source sample, our analysis of the current data set, in terms of ascertaining the relative number of objects in each evolutionary state, is necessarily limited to a plot of the distribution of spectral slope values, a .

TABLE 3
MID-INFRARED VARIABLES IN OPHIUCHUS

BKLT	Aliases	MIRLIN Flux (Jy)	ISOCAM 10.8 μm Flux (Jy)	LWS Flux (Jy)	ISOCAM 12.5 μm Flux (Jy)	Previous Ground-based Flux (Jy)
162536–241544	IRS 2	0.298 \pm 0.007	0.207 \pm 0.019			0.206 \pm 0.029 ^a
162556–242050	SR 4/IRS 12	0.810 \pm 0.020	0.541 \pm 0.023			0.994 \pm 0.029 ^a 0.75 \pm 0.14, 0.82 \pm 0.15 ^b
162603–242337	DoAr 21	0.206 \pm 0.005	0.417 \pm 0.015			0.43 \pm 0.065 ^c
162610–242056	GSS 26	1.01 \pm 0.025	0.410 \pm 0.010			0.98 \pm 0.15 ^c
162617–242023	DoAr 24/Elias 19	0.404 \pm 0.010	0.225 \pm 0.003			0.59 \pm 0.12 ^b 0.90 \pm 0.16 ^b
162621–242306	GSS 30/IRS 1	8.52 \pm 0.157	12.19 \pm 0.151			11.48 \pm 1.05 ^d
162642–242031(primary).....	Elias 26	0.410 \pm 0.010	0.287 \pm 0.005			
162644–243447	WL 12	1.05 \pm 0.020	1.97 \pm 0.025			1.74 \pm 0.26 ^c
162706–243814	WL 17			0.825 \pm 0.045	0.665 \pm 0.012	0.35 \pm 0.09 ^c
162649–243823(primary).....	WL 18	0.063 \pm 0.001	0.093 \pm 0.001	0.070 \pm 0.004	0.090 \pm 0.002	
162658–244534 ^e	SR 24	3.055 \pm 0.0563	1.885 \pm 0.101			1.95 \pm 0.04 ^a 2.9 \pm 0.55 ^b 3.95 \pm 0.26 ^f
162709–244022	GY 213			0.154 \pm 0.009	0.092 \pm 0.003	
162710–241914(primary).....	SR 21	1.73 \pm 0.043	2.255 \pm 0.018			
162711–244046.....	GY 224	0.255 \pm 0.005	0.313 \pm 0.006			0.23 \pm 0.046 ^f
162711–243832.....	WL 19	0.130 \pm 0.003	0.174 \pm 0.007	0.223 \pm 0.013	0.151 \pm 0.009	
162714–242646	IRS 33	0.062 \pm 0.001	0.109 \pm 0.006			
162715–242640	IRS 34			0.084 \pm 0.005	0.156 \pm 0.011	0.23 \pm 0.02 ^a
162715–243843 ^g	WL 20	0.411 \pm 0.010	0.491 \pm 0.006			0.18 \pm 0.03 ^c
162717–242856	GY 244	0.194 \pm 0.005	0.319 \pm 0.007			
162718–243915	GY 245	0.068 \pm 0.005	<0.013 \pm 0.001 ^h			
162718–242906	WL 4			0.400 \pm 0.023	0.275 \pm 0.010	0.18 \pm 0.03 ^c
162719–242844	WL 3	0.162 \pm 0.004	0.249 \pm 0.008	0.132 \pm 0.007	0.234 \pm 0.006	0.13 \pm 0.02 ^c
162724–244103	CRBR 85	0.216 \pm 0.005	0.277 \pm 0.009			
162726–243923	GY 262/CRBR 88	0.177 \pm 0.003	0.180 \pm 0.011			0.044 \pm 0.009 ^f
162726–244051	IRS 43	2.29 \pm 0.056	3.408 \pm 0.050			1.98 \pm 0.18 ^a
162728–243934	IRS 44	2.65 \pm 0.065	8.08 \pm 0.091			5.03 \pm 0.46 ^a
162730–242744	Elias 33/IRS 47	0.954 \pm 0.023	1.651 \pm 0.012		0.64 \pm 0.096 ^c	
162733–241115.....	GY 292/CRBR 90	0.699 \pm 0.013	0.468 \pm 0.008			0.75 \pm 0.15 ^f
162737–243035	IRS 48	3.910 \pm 0.010	6.204 \pm 0.074	2.61 \pm 0.145	6.343 \pm 0.080	5.67 \pm 0.53 ^a
162738–243658	IRS 49	0.425 \pm 0.011	0.319 \pm 0.031			0.61 \pm 0.056 ^a
162737–244238	GY 301	\leq 0.047 \pm 0.005	0.120 \pm 0.005			
162739–243914	GY 314			0.664 \pm 0.037	0.377 \pm 0.006	0.43 \pm 0.086 ^f
162745–244454	GY 344			0.117 \pm 0.007	0.077 \pm 0.003	
162747–244535	GY 352			0.073 \pm 0.004	0.039 \pm 0.005	
162751–243145	IRS 54	2.51 \pm 0.062	5.00 \pm 0.073			11.73 \pm 1.08 ^a
162755–242619	SR 10/GY 400	0.181 \pm 0.005	0.101 \pm 0.003			0.20 \pm 0.04 ^f
162923–241359	IRAS 64a	0.63/0.48 \pm 0.005				0.39 \pm 0.07 ^f

NOTE.—Table 3 is also available in machine-readable form in the electronic edition of the *Astrophysical Journal*.

^a Flux from Table 2 of Wilking et al. (1989).

^b Flux from Table 4 of Rydgren et al. (1976).

^c Flux from Table 1 of Lada & Wilking (1984).

^d Flux from Table 2 of Elias (1978).

^e The SR 24 system is a hierarchical triple, with a 6^{''}0 separation between the primary, SR 24S (=BKLT J162658–244534), and the secondary, SR 24N (=BKLT J162658–244529), which itself consists of a 0^{''}20 separation binary. Although SR 24S and SR 24N were unresolved by ISOCAM, previous ground-based observations did resolve these components. *N*-band fluxes for SR 24S are 0.78 \pm 0.029 (Wilking et al. 1989) and 2.28 \pm 0.21 Jy (Greene et al. 1994), to be compared with MIRLIN fluxes of 2.01 and 1.66 Jy for SR 24S on 1997 June 26 and 1998 June 7, respectively. *N*-band fluxes for SR 24N are 1.17 \pm 0.029 (Wilking et al. 1989) and 1.67 \pm 0.16 Jy (Greene et al. 1994), to be compared with the MIRLIN flux of 1.40 Jy for both dates of observation. Therefore, we can conclude that it is the single, primary star in this system, SR 24S, that is the MIR variable.

^f Flux from Table 1 of Greene et al. (1994).

^g WL 20 (=BKLT J162715–243843) is a triple system, which was noted as highly variable in unresolved ISOCAM 6.7 μm measurements. The previously published *N*-band flux for the WL 20 system from ground-based measurements was 0.180 \pm 0.03 Jy (Lada & Wilking 1984). Our observations resolve the triple system in the MIR and show that it is the “infrared companion,” WL 20S, that is the MIR variable (see Table 2).

^h ISOCAM data from Wilking et al. (2001).

Figure 4 shows histograms of the NIR to MIR spectral slope distributions for the young stellar population of the ρ Ophiuchi cloud core. The solid line shows the spectral slope distribution determined for the objects in our ground-based study. The spectral slopes, a , were determined using the NIR (2.2 μm)

photometry of BKLT and the MIR photometry presented in Table 2 (at 10.8 μm for MIRLIN data and at 12.5 μm for the LWS data). The dashed line shows the spectral slope distribution of objects from the ISOCAM study. Spectral slopes, a , in this case were determined from the 2.2 μm photometry of

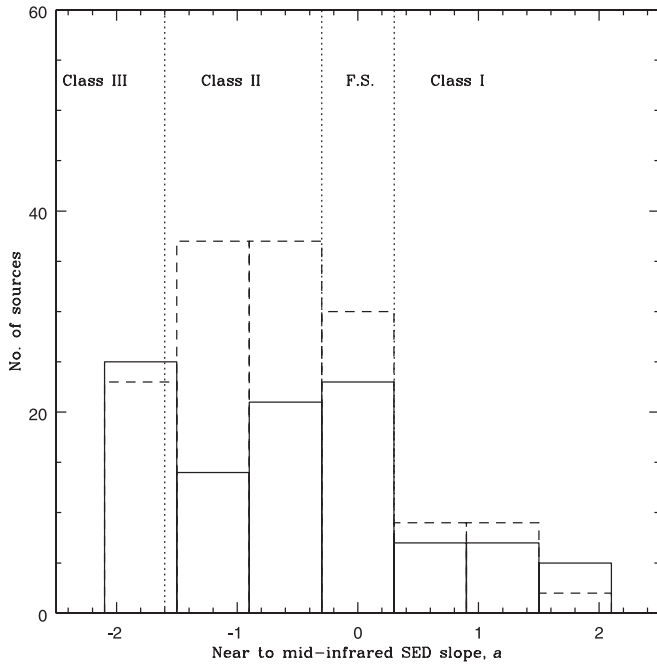


FIG. 4.—Histogram of the *observed* distribution of the NIR to MIR spectral slopes of ρ Oph embedded sources. The solid line histogram represents sources with SED slopes, a , determined using MIR data from this work; the dashed line histogram represents SED slopes determined from the $14.3 \mu\text{m}$ ISOCAM photometry. The $2.2 \mu\text{m}$ photometry of Barsony et al. (1997) was used in both cases. Note the large population of flat-spectrum ($-0.3 \leq a \leq +0.3$) objects.

BKLT and the $14.3 \mu\text{m}$ photometry from ISOCAM (Bontemps et al. 2001).

It is striking that there are more objects exhibiting flat-spectrum NIR to MIR spectral slopes, a , than Class I spectral slopes in Figure 4. The number of sources exhibiting flat-spectrum slopes is about one-half the number exhibiting Class II spectral slopes. This result holds for both the ground-based (*solid line*) and ISOCAM (*dashed line*) histograms.

Recent two-dimensional radiative transfer modeling has shown that the SEDs of flat-spectrum objects are reproduced by a central star + disk system embedded in a relatively tenuous halo (Kikuchi et al. 2002). The dusty halo in flat-spectrum objects is what is left of the remnant infall envelope with cavities carved out by outflows seen in the Class I objects. The dusty halo of flat-spectrum objects serves to heat the disk by scattering and reprocessing the central PMS star’s radiation. It is the photosphere of the warmed disk that is responsible for the large MIR to FIR excesses that produce the observed flat spectral slope observed in these objects.

The reason previous authors have neglected to remark on the large fraction of sources exhibiting flat-spectrum slopes in the ρ Oph cloud is because they had dereddened the spectral slopes assuming that these objects had intrinsic colors of T Tauri stars (Bontemps et al. 2001; Wilking et al. 2001). Such a procedure relies on the assumption that the observed source is a Class II object, seen through high foreground extinction. However, in the presence of heated and reprocessing halos, such as are present in the flat-spectrum phase, such a dereddening procedure is problematic. Complications due to heating and reprocessing of both stellar and disk radiation in the remnant infall envelopes also preclude the “dereddening” of Class I objects.

The important result here is that there is a nonnegligible phase in YSO evolution marking the transition between the Class I and Class II or Class I and young Class III phases.

During this reasonably lengthy transitional or flat-spectrum phase, a dusty halo remnant envelope remains and is slowly dispersed. Of the sources in our survey that could be assigned to SED classes based on our data, there are 19 Class I, 23 flat-spectrum, 37 Class II, and 21 Class III objects. The ISOCAM data from Tables 2–5 of Bontemps et al. (2001) contain 20 Class I, 30 flat-spectrum, 78 Class II, and 19 Class III objects (note, however, that the ISOCAM SED slopes are derived from $2\text{--}14 \mu\text{m}$). Flat-spectrum objects make up 23% and 20% of the total number of classified objects in each survey, respectively. The ratio of flat-spectrum to Class I objects is 1.2 in our survey and 1.5 in the ISOCAM survey. The typical lifetime of an object in the flat-spectrum phase is comparable to (or perhaps slightly greater than) that in the Class I phase. For a solar-luminosity object, this would correspond to 4×10^5 yr based on the study of Wilking et al. (1989).

4.2. Active Accretion and Variability at Mid-Infrared Wavelengths

Table 3 lists the objects whose fluxes, as measured in this survey, differ significantly from their published ISOCAM fluxes, or from other previously published ground-based MIR photometry. Sources are included in Table 3 if the difference between two flux measurements exceeds the quoted 3σ errors. To compile this table, we have included previously published MIR photometry, in addition to the fluxes plotted in Figures 2 and 3 (Wilking et al. 1989, 2001; Greene et al. 1994; Lada & Wilking 1984; Rydgren et al. 1976). In Table 3, the first column lists the BKLT source designation, and the second column lists a more common alias. The $10.8 \mu\text{m}$ flux and its associated error measured with MIRLIN are listed in the third column. For direct comparison, the interpolated $10.8 \mu\text{m}$ flux and its associated error from the ISOCAM data are listed in the fourth column. The $12.5 \mu\text{m}$ fluxes measured with LWS are next listed in the fifth column, and the interpolated $12.5 \mu\text{m}$ fluxes and their associated errors from ISOCAM are listed in the sixth column. Finally, the last column lists previous ground-based MIR photometry. The latter fluxes are all at $10.2 \mu\text{m}$, except for WL 17, whose $12.5 \mu\text{m}$ flux is listed.

The source of the flux discrepancies in Table 3 can be either intrinsic source variability or the presence of extended emission. Intrinsically variable sources in Table 3 are those for which fluxes from this survey exceed measured fluxes from previous surveys (all of which used larger apertures). For sources whose previous flux measurements, taken in larger apertures, exceed the fluxes from this survey, further high-resolution photometry is required to distinguish between source variability and the presence of significant extended emission. These sources are, nevertheless, included in Table 3 as possibly variable sources.

Figure 5 shows the SED slope distribution of the MIR variables and candidate variables of Table 3. Clearly, MIR variability occurs for all SED classes with optically thick disks. We have also plotted in Figure 5 the SED slope distribution of known NIR variables in ρ Oph from Table 5 of Barsony et al. (1997). NIR variability, also found for all SED classes with optically thick disks, seems to occur with somewhat higher frequency at the earlier evolutionary stages (flat spectrum and Class I). Whereas 89% of NIR variables are in the Class I or flat-spectrum stage, only 56% of the MIR variables are. This tendency must be verified from future systematic NIR and MIR variability studies to improve the statistics.

Sources exhibiting variability at both NIR and MIR wavelengths are WL 12, WL 17, WL 19, GY 244, GY 245, GY 262, and IRS 44. WL 15, an almost face-on Class I object, appears

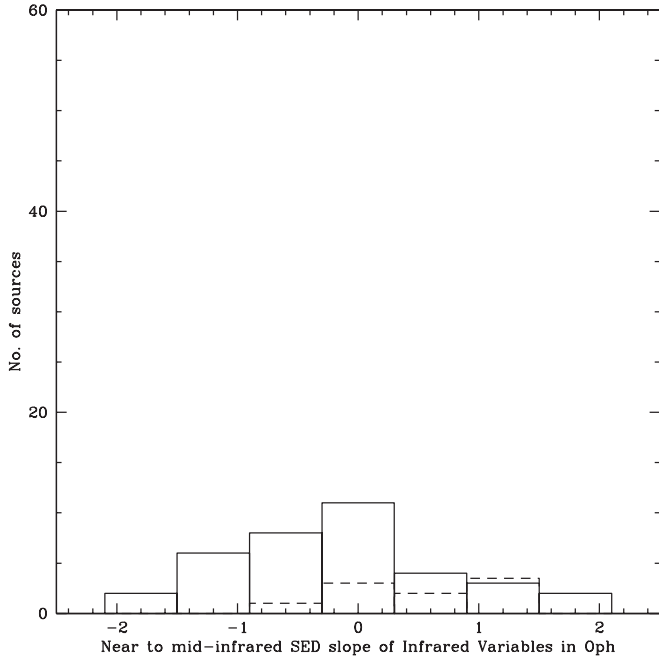


FIG. 5.—Histogram of the *observed* distribution of the NIR to MIR spectral slopes of ρ Oph variables. The solid line represents this distribution for the MIR variables of Table 3; the dashed line represents the SED distribution of the NIR variables from Table 5 of Barsony et al. (1997). Note the tendency of the NIR variables toward earlier SED classes, whereas the MIR variables seem to be evenly distributed through the SED classes with optically thick disks.

variable at NIR, but not at MIR, wavelengths. The rest of the MIR variables listed in Table 3 are apparently not highly variable at NIR wavelengths. However, further systematic variability studies in the infrared are needed to verify these preliminary results.

In order to understand what distinguishes the population of MIR variables from the rest of the embedded population in ρ Oph, we use the data compiled in Table 4 to look for a correlation between MIR variability and presence of an active accretion disk, as signaled by NIR veiling. The r_K values tabulated in Table 4 are all *spectroscopically* determined and are, therefore, reddening independent. By using moderate- ($R \sim 2000$) to high-resolution ($R \sim 20,000$) NIR spectroscopy, one can deduce the K -band “veiling” of photospheric absorption lines in a YSO by comparison with the shapes of the same absorption lines found in a spectroscopic standard star of the same spectral type. One then varies the veiling applied to the standard star’s spectrum until the veiled standard star’s spectrum best matches the YSO’s spectrum. Such a veiling measurement is independent of reddening, given the narrow wavelength range in which the relevant spectral lines lie.

The objects in Table 4 are listed in reverse NIR to MIR spectral slope (a) order, from the largest values, corresponding to Class I objects, to the smallest values, corresponding to Class III objects. The spectral slopes in Table 4 were determined using the NIR (K band, or $2.2 \mu\text{m}$) photometry of BKLT and either the $10.8 \mu\text{m}$ flux from MIRLIN or the $12.5 \mu\text{m}$ flux from LWS, as available, and as listed in Table 2.

We have excluded the known background giants from the entries in Table 4. Also excluded are the two known PAH/VSG emitters, WL 16 and WL 22. Table 4 lists the BKLT source designation in the first column and an alternate alias for each source in the second column. The K magnitude and $H - K$ color for each object are listed in the third and fourth columns, respectively, and are taken from Barsony et al. (1997), except

for the following: WL 20, GSS 30 IRS 3 (Strom et al. 1995), GY 197 (Comeron et al. 1993), WL 1 (Haisch et al. 2002), WL 18, Elias 26 (K. E. Haisch, Jr. 2003, private communication), and DoAr 24E (Chelli et al. 1988). Each object’s spectral slope, a , between 2.2 and either 10.8 or $12.5 \mu\text{m}$ (as available from Table 2), and corresponding SED class are listed in the fifth and sixth columns, respectively. Published, spectroscopically determined, K -band veiling values and visual extinctions are listed in the seventh and eighth columns, respectively.

Continuum veiling at K ($2.2 \mu\text{m}$) is quantified by the value r_K , defined as F_{excess}/F_K , where F_K is the intrinsic photospheric flux of the central object at K and F_{excess} is the amount of observed K -band flux in excess of the expected photospheric value. Veilings of $r_K \geq 0.5$ have been attributed to the presence of actively accreting circumstellar disks (Luhman & Rieke 1999; Wilking et al. 2001). Figure 6 presents a graph of the NIR to MIR spectral slopes, a , from Table 4, plotted against the *spectroscopically determined* r_K values published by various authors (Greene & Meyer 1995; Wilking et al. 1999; Luhman & Rieke 1999; Barsony et al. 2002; Greene & Lada 2002; Prato et al. 2003; Doppmann et al. 2003; G. Doppmann 2004, private communication). The horizontal dashed line in Figure 6 denotes the boundary between optically thick (above the line) and optically thin (below the line) disks, at $r_K = 0.58$ (Wilking et al. 2001). Class I objects generally exhibit $r_K \geq 1$ (the one exception being GY 91/CRBR 42 with $r_K = 0.3$). Flat-spectrum objects generally have $r_K \geq 0.58$ (with the exception of GY 244, with $r_K = 0$). Class II objects have the widest range of r_K values, ranging from $0 \leq r_K \leq 4.5$ (the record of 4.5 being held by Elias 26). Class III objects clearly have optically thin disks, most with $r_K = 0$. The most striking feature of this graph is the highly variable value of veiling that a single source can exhibit in any of the SED classes in which active disk accretion can take place (i.e., in the Class II/flat-spectrum/Class I phases). This is direct observational evidence for highly time-variable accretion activity in disks.

4.3. Disk Structures

A current problem of great interest is how disks are dissipated in YSOs. Is it possible that disk winds would preferentially clear the innermost portions of a disk before the outer portions, or vice versa? One possible way to address this question is to look for the frequency of NIR versus MIR excesses, perhaps as a function of the age of the system, since NIR excesses originate from disk regions much closer to the central object than MIR excesses.

For this purpose, we consider only those Class II and Class III objects whose effective temperatures have been spectroscopically determined and that have good estimates of A_V . We have omitted the known binaries, S1, SR 24N, WL 13, Elias 34, IRS 2, and GSS 29 (Barsony et al. 2003; G. Doppmann 2004, private communication), from this plot. These systems would either be unresolved by our MIR data (spectroscopic binaries) or their projected angular separations are so small that both of their spectra would fall into a single slit, thereby invalidating the derived effective temperature and visual extinction values. Individual components of well-resolved multiple systems have been included in Figure 7, however.

We calculate K -band excesses, ΔK , and N -band excesses, ΔN , defined as the logarithm of the ratio of the observed flux to the flux expected from the PMS star’s photosphere at 2.2 and $10.8 \mu\text{m}$, respectively, seen through the appropriate amount of foreground extinction. More specifically, we use the definitions $\Delta K = \log F(\text{observed})_{2.2 \mu\text{m}}/F(\text{photospheric})_{2.2 \mu\text{m}}$ (Strom et al. 1989) and $\Delta N = \log F(\text{observed})_{10.8 \mu\text{m}}/F(\text{photospheric})_{10.8 \mu\text{m}}$

TABLE 4
 ρ OPH SOURCE PROPERTIES

BKLT	Aliases	K (mag)	$H - K$ (mag)	α_{IR}^a	SED	r_K^b	A_V^b (mag)
162722–242939	GY 256	12.75	2.79	+2.35	I
162751–243145	IRS 54	10.87	2.63	+1.77	I	>2	...
162724–244103	CRBR 85	13.21	≥ 2.29	+1.59	I
162715–243843	WL 20						
	WL 20S	12.57	1.88	+1.38	I	<0.9 (BGB02)	41.3 (BGB02)
162709–243718	WL 15	7.54	4.47	+1.27	I	>2	11.1–17.0 (B02)
162729–243917	IRS 46/YLW 16B	11.46	3.19	+1.15	I	>1	...
162617–242347	CRBR 12	12.04	3.54	+1.15	I	2.0 (D04)	...
162728–243934	IRS 44/YLW 16A	9.65	3.44	+1.10	I	1, 2.2 (D04)	...
162621–242306	GSS 30 IRS 1/GY 6	8.32	2.51	+1.04	I	>2	...
162640–242715	GY 91/CRBR 42	12.51	≥ 2.99	+0.98	I	0.3 (D04)	...
162726–244051	IRS 43/GY 265	9.46	3.71	+0.90	I	3 (GL02), 1.7 (PGS03)	38 (PGS03)
162644–243447	WL 12	10.18	2.89	+0.88	I	1–3	...
162721–242953	WL 6	10.04	4.35	+0.76	I	>4.6 (GL02)	...
162706–243814	WL 17	10.28	3.29	+0.60	I	3.9 (D04)	...
162630–242258	GY 51/VSSG 27					2.0, 0.5, 2.3 (GM95)	22 (GM95)
	GY 51/VSSG 27 SW(primary)	11.14	3.59	+0.46	I		
162610–242056	GSS 26	9.38	2.25	+0.34	I	4, 0.75	21.3
162745–244454	GY 344	11.84	2.21	+0.30	F.S.
162726–244246	GY 260	12.54	3.17	+0.28	F.S.
162719–242844	WL 3	11.20	3.29	+0.24	F.S.	1.0 (GM95)	...
162714–242646	IRS 33/GY 236	12.23	3.04	+0.23	F.S.
162721–244142	IRS 42	8.41	2.90	+0.22	F.S.	>1	...
162717–242856	GY 244	10.95	2.95	+0.21	F.S.	0	...
162711–244046	GY 224	10.79	2.90	+0.21	F.S.	>0.5	...
162648–242840	WL 2S (primary)	10.99	2.06	+0.21	F.S.	1.5 (GM95)	...
162709–244022	GY 213	11.32	2.17	+0.19	F.S.
162718–243915	GY 245	11.98	3.45	+0.15	F.S.
162739–244316	IRS 51	8.93	3.49	+0.13	F.S.	1–3	~33.7
162711–243832	WL 19	11.23	>4.27	+0.12	F.S.	3.7 (D04)	...
162618–242416	CRBR 15	11.94	1.95	+0.09	F.S.	0.64(WGM99)	17.7
162623–242441	GY 21(secondary)	9.94	1.69	+0.08	F.S.	1, 2.5 (GM95)	13.5, 16 (GL97)
162737–243035	IRS 48	7.42	1.23	+0.05	F.S.
162730–242755	Elias 33/GY 279/VSSG 17	8.95	2.69	+0.05	F.S.	0.75, 1, 2.8 (GM95), 0.5 (D04)	24.5, 28 (GL97)
162715–242640	IRS 34	10.66	2.81	–0.03	F.S.	1.8 (GM95)	...
162741–244337	GY 323	11.93	2.56	–0.14	F.S.
162623–242101	DoAr 24E/Elias 22						
	DoAr 24E/Elias 22(secondary)	7.81	1.59	–0.14	F.S.	...	16.2
162728–242721	IRS 45/VSSG 18	9.39	2.09	–0.22	F.S.	0	17.7
162637–242302	GY 81/VSSG 4	10.92	1.91	–0.26	F.S.	1–2	16.3
162619–242820	Elias 20/VSSG 1	8.68	2.08	–0.27	F.S.
162607–242725		10.48	2.02	–0.30	F.S.
162704–242716	GY 195	11.30	2.25	–0.34	II
162732–243235	GY 291	10.89	1.90	–0.37	II
162726–244045	GY 263	11.93	2.76	–0.40	II
162624–242449	Elias 23/GY 23 (primary)	7.20	1.48	–0.40	II	0.75, 1.2 (DJW03)	11
162704–242830	WL 1						
	WL 1S(primary)	10.76	2.08	–0.46	II	0.8 (D04)	...
162648–242836	WL 2N (secondary)	12.48	3.25	–0.46	II
162726–243923	GY 262	9.77	2.30	–0.53	II	1	22.7
162739–243914	GY 314	8.35	0.92	–0.55	II	0.5, 1.9(GM95)	7.1, 4.9 (GM95)
162658–244534	SR 24S(primary)	7.08	1.17	–0.56	II	1–3, 0.1(GM95)	4.3
162747–244535	GY 352	11.04	1.83	–0.59	II
162718–242906	WL 4	9.13	1.93	–0.59	II	0.25, 1.1(GM95)	19
162658–244529	SR 24N(secondary)	7.42	1.18	–0.59	II	2, 0.1(GM95)	7
162624–241616	Elias 24	6.77	1.46	–0.59	II	1–3, 4.5 (DJW03)	8.2
162712–243449	WL 11	11.53	1.76	–0.63	II
162645–242309	Elias 27	8.88	1.62	–0.67	II	0.75, 1.8(GM95)	17, 14 (GM95)
162704–242830	WL 1						
	WL 1N(secondary)	10.85	2.06	–0.70	II
162733–241115	GY 292/CRBR 90	7.92	1.37	–0.75	II	1, 4.0 (DJW03)	10.3
162642–243103	WL 7	10.73	2.48	–0.75	II
162738–243658	IRS 49/GY 308	8.31	1.24	–0.83	II	0.75, 1.6 (DJW03)	10.3

TABLE 4—Continued

BKLT	Aliases	K (mag)	$H - K$ (mag)	α_{IR}^a	SED	r_K^b	A_V^b (mag)
162715–243843	WL 20						
	WL 20E	10.13	1.15	−0.83	II	0.2 (BGB02)	16.3 (BGB02)
162642–242031	Elias 26						
	Elias 26(primary)	8.30	0.85	−0.85	II	0.06 (PGS03)	11 (PGS03)
162649–243823	WL 18						
	WL 18S(primary)	10.21	1.35	−0.93	II	>1	9.2
162715–243843	WL 20						
	WL 20W	10.40	1.18	−0.94	II	0.2 (BGB02)	16.3 (BGB02)
162617–242023	Elias 19/GSS 28	8.09	0.58	−0.98	II	0.5, 0.1(GM95), 1.2 (DJW03)	2.8
162616–242225	Elias 18/GSS 29	8.19	1.04	−0.98	II	0, 0.1(GM95), 0.3 (DJW03)	10.6, 12 (GM95)
162718–242853	WL 5	10.28	4.04	−1.01	II	0 (GM95)	51 (GM95)
162536–241544	IRS 2	8.36	0.70	−1.02	II	0, 0.1(GM95)	6.7
162556–242050	SR 4	7.25	0.72	−1.03	II	1.5, 2, 3.7 (DJW03)	1.8
162755–242619	SR 10/GY 400	8.74	0.60	−1.11	II	0.5	0
162710–241914	SR 21N(primary)	6.30	1.03	−1.11	II	0.78 (PGS03)	9 (PGS03)
162709–243408	WL 10	8.85	1.39	−1.12	II	0.75, 0.6 (D04)	12.8
162727–243116	WL 13/VSSG 25	9.30	1.11	−1.26	II	0.25, 0.5(GM95)	11
162642–243325	WL 8	9.44	3.05	−1.28	II
162623–242101	DoAr 24E/Elias 22						
	DoAr 24E/Elias 22(primary)	7.06	0.67	−1.31	II	0, 1.6 (DJW03)	6.4
162740–242205	SR 9/Elias 34	7.20	0.51	−1.46	II	0.75	0
162646–241203	VSS 27	7.51	0.82	−1.54	II	0.75	6.7
162623–242603	DoAr 25/GY 17	7.57	0.79	−1.56	II	0, 0.1(GM95)	0
162923–241359	WLY 64/IRAS 64a ^c	6.45	0.91	−1.65	III
162603–242337	Elias 14/DoAr 21	6.16	0.59	−2.53	III	0	5.7
162609–243411	SR 3	6.42	0.49	−2.58	III	0	8.2
162634–242330	Elias 25/S1/GY 70	6.32	0.96	−3.16	III	0	10 (BA92)
	GSS 30 IRS 3 /LFAM 1	13.79	...	≤+1.55
	GY 197/LFAM 26	14.80	≥3.10	≤+1.48	...	1.2 (D04)	...
162631–243141	IRS 15/GY 58	13.35	1.46	≤+0.86
162803–243441	GY 450	13.09	2.32	≤+0.71
162542–242712	IRS 7	12.94	0.79	≤+0.67
162737–242846	GY 303	12.68	1.84	≤+0.66
162728–243143	GY 272	13.72	1.78	≤+0.64
162622–242409	GY 11	14.15	1.22	≤+0.64
162654–242703	GY 154	12.91	2.13	≤+0.53	25 (W01)
162703–242615	GY 188	12.52	≥2.98	≤+0.47
162904–244057		12.79	2.28	≤+0.42
162804–243451	GY 461	12.65	2.46	≤+0.42
162705–242036	GY 200	12.93	1.67	≤+0.41
162706–242837	GY 202	12.97	1.70	≤+0.39	...	0.5 (WGM99)	13 (WGM99)
162628–242153	GY 38	12.93	2.60	≤+0.39
162608–241855	CRBR 4	12.79	≥2.71	≤+0.38
162724–244147	GY 258	12.65	2.40	≤+0.36
162653–243236	GY 146	13.18	2.32	≤+0.30
162622–242721	GY 14	12.44	2.06	≤+0.23
162836–243552		10.37	1.74	≤+0.23
162732–242943	GY 287	12.95	2.23	≤+0.23
162732–243242	GY 290	13.03	2.85	≤+0.18
162620–242840		11.71	1.61	≤+0.16
162715–243054	CRBR 70/IRS 35	12.73	≥2.77	≤+0.13
162727–243217	GY 266	12.28	2.48	≤+0.05
162730–243335	GY 278	12.31	3.26	≤+0.05
162625–242325	GY 31	13.09	3.98	≤+0.05	56 (WGM99)
162729–243408	GY 275	12.79	2.01	≤0.00
162715–242514	IRS 36/GY 241	13.18	≥2.32	≤−0.03
162656–242838	GY 163	12.66	2.28	≤−0.05	32 (WGM99)
162648–242626	GY 130	12.79	2.67	≤−0.07
162749–242522	GY 371	10.17	1.04	≤−0.12
162622–242449	CRBR 23	12.97	2.25	≤−0.14
162629–241908	SKS 1–19/LFAM 8	11.19	2.05	≤−0.22	...	0	23.4
162642–242627	GY 101	12.58	≥2.92	≤−0.24
162709–242955	GY 215	12.93	2.57	≤−0.25
162657–243538	WL 21	12.67	2.18	≤−0.27
162724–242929	GY 257	12.25	2.71	≤−0.38

TABLE 4—Continued

BKLT	Aliases	K (mag)	$H - K$ (mag)	$\alpha_{\text{IR}}^{\text{a}}$	SED	r_K^{b}	A_V^{b} (mag)
162641–241801		11.63	2.25	≤ -0.38
162746–243759	GY 346	12.29	1.48	≤ -0.45
162737–244238	GY 301	11.30	3.47	≤ -0.48
162522–243452		12.54	2.50	≤ -0.52
162721–242151	GY 255	10.96	1.71	≤ -0.53
162631–243105	IRS 14	10.80	1.56	≤ -0.54
162724–242935	GY 259	12.41	2.64	≤ -0.55
162750–244822	WLY 54	8.23	0.98	≤ -0.62
162710–243322	WL 9	11.86	2.11	≤ -0.62
162732–244500	GY 288	13.13	2.74	≤ -0.62
162705–242619	IRS 30/GY 203	11.05	2.52	≤ -0.76
162649–243823	WL 18						
	WL 18N(secondary)	12.05	1.32	≤ -0.76
162625–242446	GY 29	10.86	2.11	≤ -0.79	...	0	22.3
162642–242031	Elias 26						
	Elias 26(secondary)	9.56	0.90	≤ -0.80	...	0.22 (PGS03)	14 (PGS03)
162654–242231	GY 156	10.19	1.78	≤ -0.82	...	0	21.6
162630–242258	GY 51/VSSG 27					2.0, 0.5, 2.3 (GM95)	22 (GM95)
	GY 51/VSSG 27 NE(secondary)	11.62	2.87	≤ -0.85	...		
162718–242427	GY 248	11.12	2.13	≤ -0.88
162732–243323	GY 289	10.71	1.97	≤ -0.93	23 (W01)
162659–243556	WL 14	11.74	1.64	≤ -0.96	...	0	18
162654–242622	GY 153/VSSG 5	9.88	1.82	≤ -0.98	...	0.25, 0.1 (GM95)	21
162728–241709		12.82	2.04	≤ -0.99
162719–244139	SR 12	8.41	0.28	≤ -0.99	...	0	0.7, 1.7 (BA92)
162738–243043	IRS 50/GY 306	9.59	1.01	≤ -1.01	...	0	11
162701–242138	GY 181	9.32	1.74	≤ -1.15
162642–242633	GY 103	12.52	≥ 2.98	≤ -1.15
162711–242343	IRS 32/GY 228	10.06	1.58	≤ -1.17
162743–244309	IRS 53/GY 334	11.17	2.76	≤ -1.19
162618–242310	CRBR 17	12.32	2.64	≤ -1.30
162722–241759	VSSG 22	9.41	1.38	≤ -1.44	...	0	16.3
162841–241618		11.61	2.92	≤ -1.50
162655–242030	GSS 41/GY 157	9.69	2.13	≤ -1.53
162643–241635	IRS 19/VSSG 11	9.58	1.27	≤ -1.61	III	0	14.2, 10 (BA92)
162615–241924	CRBR 9	9.98	1.46	≤ -1.62	III	0	16.3
162547–241833	IRS 8	9.69	1.08	≤ -1.63	III
162721–244335	GY 253	10.78	2.53	≤ -1.69	III	0	29
162804–243459	GY 463	10.92	2.48	≤ -1.81	III
162752–244049	IRS 55/GY 380	8.09	0.60	≤ -1.90	III
162557–243032	IRS 13/GSS 20	8.37	0.63	≤ -1.94	III	0, 0.1 (GM95)	3.2, 4.3 (BA92)
162710–241921	SR 21S(secondary)	9.25	0.75	≤ -1.98	III	0.15 (PGS03)	9.3 (PGS03)
162618–241712		11.45	2.05	≤ -2.01	III
162738–242528	GY 309	12.73	2.91	≤ -2.07	III
162549–243139	IRS 9	9.41	1.21	≤ -2.11	III
162550–243913	IRS 10	8.24	0.45	≤ -2.21	III
	SR-2	7.82	0.09	≤ -2.67	III	...	0.51 (W94)
162746–242323	Elias 35/GY 351 ^d	7.29	1.12	≤ -2.74	M0 III

NOTE.—Table 4 is also available in machine-readable form in the electronic edition of the *Astrophysical Journal*.

^a Parameter α_{IR} is calculated between 2.2 and either 10.8 or 12.5 μm , as available from Table 2.

^b A_V and r_K values are from Luhman & Rieke (1999), unless otherwise indicated.

^c The nature of WLY 64 remains to be clarified, although it is listed as an FU Ori candidate source by Luhman & Rieke (1999).

^d Spectroscopically determined background giant (Luhman & Rieke 1999).

REFERENCES.—B02 = Boogert et al. 2002; BA92 = Bouvier & Appenzeller 1992; BGB02 = Barsony et al. 2002; DJW03 = Doppmann et al. 2003; D04 = G. Doppmann 2004, private communication; GL97 = Greene & Lada 1997; GL02 = Greene & Lada 2002; GM95 = Greene & Meyer 1995; PGS03 = Prato et al. 2003; W94 = Walter et al. 1994; W01 = Wilking et al. 2001; WGM99 = Wilking et al. 1999.

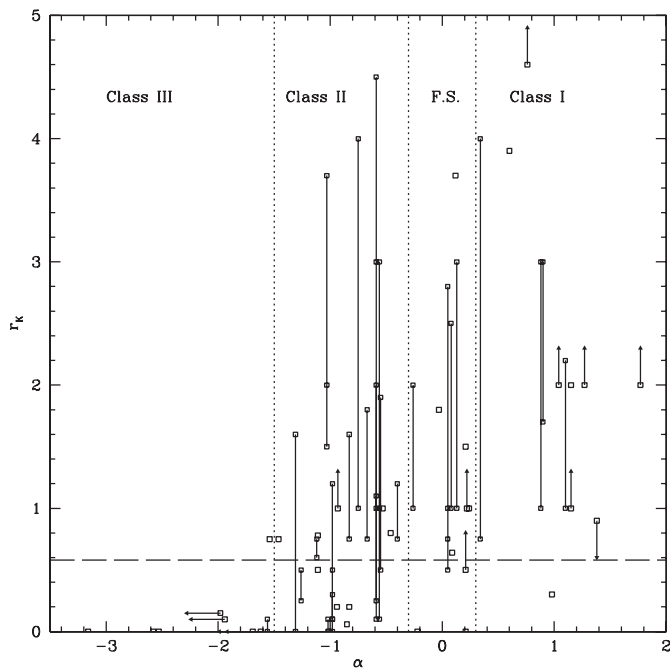


FIG. 6.—Plot of the K -band veiling (r_K values) vs. the SED slopes, α , for ρ Oph embedded sources from Table 4. Note that large variability in K -band veiling is a ubiquitous phenomenon among all SED classes with optically thick disks. This is a robust result, withstanding any errors that may have been introduced by the use of nonsimultaneous NIR and MIR photometry in the determination of the plotted SED slopes. The horizontal dashed line, drawn at $r_K = 0.58$, indicates the dividing line between optically thick (above the line) and optically thin (below the line) disks (Wilking et al. 2001).

(Skrutskie et al. 1990). Note that this method of calculating r_K is reddening dependent, since it results in a different ΔK value for a different input A_V , in contrast to the spectroscopically determined values of r_K used in Figure 6.

Figure 7 shows the resulting ΔN versus ΔK plot. In the left panel, the expected photospheric contributions at K and N were determined assuming a blackbody radiator at the spectroscopically determined effective temperature for each source. In the right panel, Kurucz model atmospheres of the appropriate temperature, with solar abundances and $\log g = 3.5$, were used to infer the photospheric emissions at K and N . Class III objects are plotted by triangles, and Class II objects by squares. The demarcations between optically thin/thick disks at $\Delta K = 0.2$ and at $\Delta N = 1.2$ are indicated by the dashed and dotted lines, respectively (Skrutskie et al. 1990).

Class III objects, as expected, have optically thin disks at both NIR and MIR wavelengths, with ΔK values scattered about 0.0 (for the blackbody models). There is an inherent bias in the sample of Class III objects plotted in Figure 7, since in order to appear on this plot, they are all detected in the MIR. Therefore, instead of being scattered about a mean $\Delta N = 0.0$, there appears to be a positive bias in the ΔN values of these Class III objects.

The sample of Class III objects plotted here are unique in that they have any detectable MIR emission above photospheric at all, signaling the presence of surrounding disks, even though these are optically thin. These seem to have been cleared possibly from inside out (ΔK consistent with photospheric emission only, but ΔN above photospheric).

The dramatic finding in Figure 7 is the lack of any objects occupying the lower right quadrant of each plot, corresponding to optically thick inner disks with optically thin outer disks,

for both the blackbody and Kurucz model central objects. This finding is consistent with two possible disk dissipation scenarios: either disk clearing proceeding at the same rate at all radii or disk clearing from the inside out. For the case of disk clearing proceeding at the same rate at all radii, we would expect to see a clear correlation between ΔK and ΔN , whereas for disk clearing from the inside out, we would expect all of the quadrants of Figure 7, except the lower right, to be significantly populated.

At first sight, it may seem as though there is a correlation between ΔK and ΔN , in the left panel of Figure 7, with the exception of GY 11. However, the sources GY 314, GSS 29, and GSS 39 have been previously pointed out as examples of disks with inner holes (Wilking et al. 2001), which should occupy the upper left quadrant in each panel of Figure 7. In fact, GY 314 does lie in the upper left quadrant of each panel of Figure 7, whereas GSS 39 lies no further than $\Delta N = 0.1$ from this quadrant even in the case of a blackbody model for the central object (GSS 29 is a newly discovered spectroscopic binary and has been excluded from Fig. 7 on that basis). If we allow an error of just $\Delta N = 0.1$ in the MIR excess determinations for the blackbody models, then the upper two quadrants for both central source models would be equally occupied, and one could argue for evidence for disk clearing from the inside out.

Of course, were we to consider only the right panel, where Kurucz model atmospheres have been used to model the central objects, we would conclude that disk clearing does proceed from the inside out. However, we must point out a systematic error that seems to be present in the NIR excesses as determined when using Kurucz model atmospheres for the central objects: instead of being equally distributed about a $\Delta K = 0$ value, as would be expected for random errors for lack of NIR excess emission, the objects with optically thin disks are scattered about a mean negative value of $\Delta K = -0.1$. This systematic error could be caused by the presence of just 10%–20% veiling at J band, or by the presence of some scattered light at J .

To definitively decide on the disk clearing mechanism, two avenues of further investigations are called for. First, spectral type determinations for more Class II and Class III sources are needed, in particular, ones for which the K - and N -band fluxes are known, in order to improve the statistics of Figure 7. Secondly, detailed investigations of the contributions to each individual object's J -band flux from scattering and/or veiling are needed, in order to more accurately determine the K -band excesses when using Kurucz model atmospheres.

4.4. Effect of Multiplicity on Disk Evolution

Table 5 lists the targets observed in our MIR survey that are known to be in multiple systems (Barsony et al. 2003). Of a total of 22 multiple systems observed, 2 were new discoveries: IRS 34, at $0''.31$ separation, and WL 1, at $0''.82$ separation. Fifteen of the observed, known multiple systems were resolved in this study. Individual component fluxes and/or flux upper limits are listed in Table 5.

Data from this survey have been used to study the multiplicity frequency among Class I protostars, with the result that the restricted companion fraction for the observed magnitude difference and separation range is consistent with that found for Class II objects. Thus, the restricted companion fraction for both Class I and Class II objects exceeds that found for main-sequence stars by a factor of 2 (Haisch et al. 2002, 2004). These authors also inferred that many subarcsecond Class I binaries remain to be discovered.

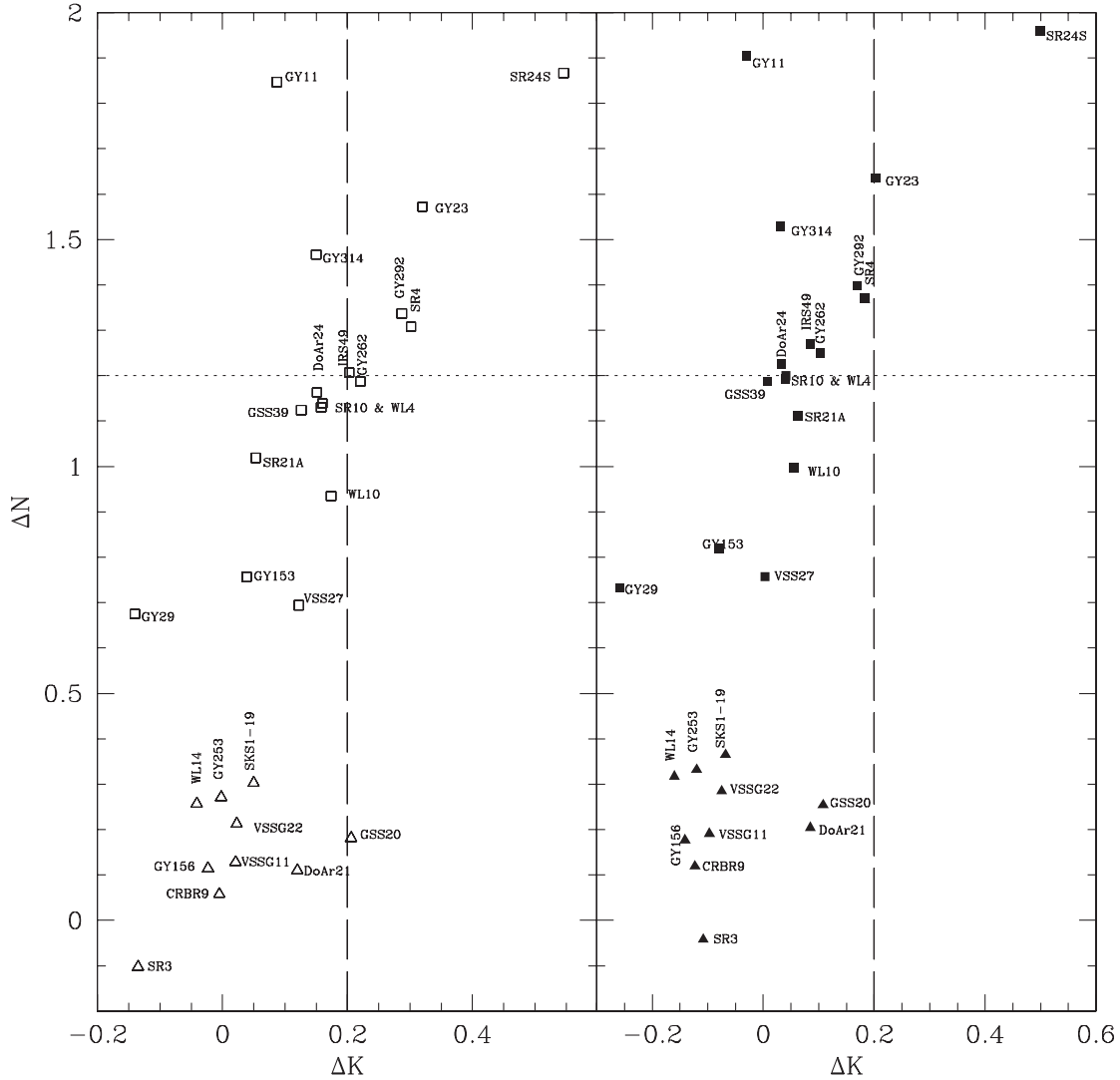


FIG. 7.—Plot of excess emission (above photospheric) at NIR (ΔK) and MIR (ΔN) wavelengths for Class II objects (*squares*) and Class III objects (*triangles*) for which spectroscopic T_{eff} measurements are available. The vertical dashed line at $\Delta K = 0.2$ indicates the boundary between optically thick ($\Delta K \geq 0.2$) and optically thin ($\Delta K \leq 0.2$) inner disks. The horizontal, dotted line at $\Delta N = 1.2$ indicates the boundary between optically thick ($\Delta N \geq 1.2$) and optically thin ($\Delta N \leq 1.2$) disk regions farther out. In the left panel, with open symbols, blackbody emission was used to model the central YSO, whereas in the right panel, with filled symbols, Kurucz model atmospheres of the appropriate effective temperature were used to model the central YSO.

The question of how binarity affects disk evolution may be divided into several categories, based on binary separation (Looney et al. 2000). Gravitationally bound objects evolving from separate envelopes (≥ 6500 AU separation), objects with separate disks but common envelopes ($100 \text{ AU} \leq r \leq 6500 \text{ AU}$), and objects sharing both a single disk and a single envelope (≤ 100 AU separation) must evolve differently. The angular scales accessible in this survey are most amenable for studies of multiple systems that have separate disks but common envelopes.

A detailed study of an unusual triple system, WL 20, that was part of this survey has shown that disk-disk interaction has resulted in enhanced accretion onto one component of this system, WL 20S. This tidally induced disk disturbance explains the Class I SED of this object, although it is coeval, at an age of several million years, with its Class II SED companions (Ressler & Barsony 2001; Barsony et al. 2002).

A comprehensive study of disk evolution in these multiple systems requires both spatially resolved, multiwavelength, NIR photometry (a challenge at subarcsecond separations and at the faint J magnitudes of many of these systems) and spatially

resolved NIR spectroscopy. Such data have been obtained for a dozen binary systems, and their analysis is the subject of a future work (M. Barsony et al. 2005, in preparation).

5. SUMMARY

We have carried out a high spatial resolution, ground-based, MIR imaging survey of 172 objects toward the ρ Ophiuchi star-forming cloud core. The target list included 102 objects chosen for their combined properties of infrared brightness ($K \leq 13.0$) and red color ($H - K \geq 1.67$) from the NIR survey of Barsony et al. (1997), augmented by known cloud members inferred from observations at other wavelengths.

Eighty-five of the target objects were detected. The general agreement between the MIR fluxes determined in this study with the ISOCAM-determined fluxes for objects common to both surveys is quite good, as is the agreement for objects in common to both studies for which only ground-based flux upper limits could be determined. A significant fraction of sources (18 objects) were found to be MIR variables, and a further 19 objects are either extended and/or variable.

TABLE 5
MID-INFRARED OBSERVATIONS OF KNOWN BINARY/MULTIPLE SYSTEMS IN OPHIUCHUS

BKLT	Alias	α (J2000.0)	δ (J2000.0)	System Type ^a	Separation (arcsec)	P.A. ^b (deg)	Resolved in MIR?
162536–241544	ROX 1	16 25 19.28	–24 26 52.1	B	0.236	156	N
162623–242101	IRS 2	16 25 36.75	–24 15 42.1	B	0.44 ± 0.03	79 ± 4	N
162623–242101	DoAr 24E	16 26 23.38	–24 20 59.7	B	2.05	148.6	Y
162624–242449	Elias 23+GY 21	16 26 24.06	–24 24 48.1	B	10.47	322.6	Y
162623–242441	Elias 23	16 26 24.06	–24 24 48.1				
162623–242441	GY 21	16 26 23.60	–24 24 39.4				
162630–242258	VSSG 27	16 26 30.50	–24 22 57.1	B	1.22 ± 0.03	68 ± 1	Y
162634–242330	S1	16 26 34.18	–24 23 28.2	B	0.020	110	N
162642–242031	GSS 37	16 26 42.87	–24 20 29.8	B(T?)	1.44	67.0	Y
162646–241203	VSS 27	16 26 46.44	–24 12 00.0	B	0.59	104.6	N
162648–242840	WL 2	16 26 48.50	–24 28 38.7	B	4.17	343	Y
162648–242836	WL 2(A)	16 26 48.50	–24 28 38.7				
162648–242836	WL 2(B)	16 26 48.42	–24 28 34.7				
162649–243823	WL 18	16 26 48.99	–24 38 25.1	B	3.55	293	Y
162658–244534	SR 24	16 26 58.52	–24 45 36.7	T	5.093	60	Y
162658–244529	SR 24A	16 26 58.52	–24 45 36.7				
162658–244529	SR 24B	16 26 58.45	–24 45 31.7		0.197	84	N
162704–242830	WL 1	16 27 04.12	–24 28 29.9	B	0.82	321.2	Y
162710–241914	SR 21	16 27 10.28	–24 19 12.6	B	6.33	175	Y
162710–241921	SR 21A	16 27 10.28	–24 19 12.6				
162710–241921	SR 21B	16 27 10.33	–24 19 18.9				
162715–242640	IRS 34	16 27 15.48	–24 26 40.6	B	0.31	236	
162715–243843	WL 20	16 27 15.69	–24 38 43.4	T			
162715–243843	WL 20W	16 27 15.69	–24 38 43.4		3.17 (east-west separation)	270	Y
162715–243843	WL 20S	16 27 15.72	–24 38 45.6		2.26 (south-west separation)	173	Y
162715–243843	WL 20E	16 27 15.89	–24 38 43.4		3.66 (south-east separation)	232	Y
162719–244139	SR 12+IRS 42	16 27 19.55	–24 41 40.0	T			
162719–244139	SR 12	16 27 19.55	–24 41 40.0	B	0.30	85	N
162721–244142	IRS 42	16 27 21.45	–24 41 42.8	B	26.8	85.8	Y
162726–244045	GY 263+IRS 43	16 27 26.63	–24 40 44.9	B	6.99	322	Y
162726–244051	GY 263	16 27 26.63	–24 40 44.9				
162726–244051	IRS 43	16 27 26.94	–24 40 50.				
162726–243923	IRS 44+GY 262	16 27 26.49	–24 39 23.0	T(?)			Y
162726–243923	GY 262	16 27 26.49	–24 39 23.0		23.21		
162728–243934	IRS 44	16 27 28.01	–24 39 33.6	B	0.27	81	N
162727–243116	WL 13	16 27 27.40	–24 31 16.6	B	0.46	356	N
162730–242744	VSSG 17	16 27 30.17	–24 27 43.5	B	0.25	26	N
162740–242205	SR 9	16 27 40.28	–24 22 04.3	B	0.59	350	N
162752–244049	ROXs 31	16 27 52.07	–24 40 50.4	B	0.39	71.6	N

NOTES.—Units of right ascension are hours, minutes, and seconds, and units of declination are degrees, arcminutes, and arcseconds. Table 5 is also available in machine-readable form in the electronic edition of the *Astrophysical Journal*.

^a B = binary; SpB = spectroscopic binary; T = triple; Q = quadruple.

^b Position angles are east of north, measured from the primary at K , except for IRS 34, where the primary is at N , since no resolved K -band data exist.

A plot of the frequency of NIR to MIR spectral slopes, a , for the objects with newly determined MIR fluxes shows 19 Class I, 23 flat-spectrum, 37 Class II, and 21 Class III objects. It is argued that flat-spectrum objects represent a distinct evolutionary phase in which the remnant infall envelopes from the Class I phase are dispersed and that YSOs spend a significant fraction of time, of order 4×10^5 yr, in this state.

A plot of the spectroscopically determined NIR veiling, r_K , versus NIR to MIR spectral slope, a , for the detected objects in our survey for which published r_K values are available is presented. We find a general trend of an increasing r_K threshold with increasing a , such that Class I objects generally exhibit $r_K \geq 1$, flat-spectrum objects generally have $r_K \geq 0.58$, and Class III objects generally have $r_K = 0$. Class II objects, however, have the widest range of r_K values, from $0 \leq r_K \leq 4.5$. The most striking result, however, is the highly variable value

of veiling that a single source can exhibit in any of the Class II/flat-spectrum/Class I phases, signaling the highly time-variable accretion activity in disks.

Finally, to study disk dispersal mechanisms, we present plots of ΔN (MIR excess above photospheric emission) versus ΔK (NIR excess above photospheric emission), for two photospheric models: blackbody and Kurucz model atmospheres. Determinations of the MIR and NIR excesses were made for the subset of our MIR survey sample for which spectroscopically determined effective temperatures and reliable, previously published A_V values are available. In all cases, we find no sources occupying the region of the plot that corresponds to optically thick inner disks with optically thin outer disks. By contrast, the entire region of optically thin inner disks, spanning the range from optically thin to optically thick outer disks, is populated, as is the region with both optically thick inner and outer disks.

The results are consistent with disk dispersal proceeding from the inside out, but further observational investigations to confirm this hypothesis are suggested.

This paper is dedicated to the memory of a dear friend, colleague, and MIR astronomer extraordinaire, Lynne K. Deutsch, who passed away after a long illness on the night of 2004 April 2.

Financial support through NSF grants AST 00-96087 (CAREER), AST 97-53229 (POWRE), AST 02-06146, the NASA/ASEE Summer Faculty Fellowship program at the Jet Propulsion Laboratory, and NASA's Faculty Fellowship Program at Ames Research Center has made the completion of this work possible. We wish to thank the staff at the Keck and Palomar observatories for their enthusiasm, patience, and assistance in making it

possible to use MIRLIN at these telescopes and Bob Goodrich for his support with the LWS instrument at Keck I. Development of MIRLIN was supported by the JPL's Director's Discretionary Fund, and its continued operation was funded by an SR+T Award from NASA's Office of Space Science.

Suzanne Casement, former postdoctoral researcher at U.C. Riverside, Ana Matkovic, former summer undergraduate researcher at Harvey Mudd College, and former HMC undergraduate, Christian Baude, also contributed during the early data reduction phases of this work. Patricia Monger's contributions in systems administration and in providing the plotting program, SM, have been invaluable and are gratefully acknowledged. We thank the referee, Bruce Wilking, for his meticulous readings of the manuscript and for his numerous helpful suggestions for its improvement.

REFERENCES

- Armitage, P. J., Clarke, C. J., & Palla, F. 2003, *MNRAS*, 342, 1139
 Barsony, M., Greene, T. P., & Blake, G. A. 2002, *ApJ*, 572, L75
 Barsony, M., Kenyon, S. J., Lada, E. A., & Teuben, P. J. 1997, *ApJS*, 112, 109
 Barsony, M., Koresko, C., & Matthews, K. 2003, *ApJ*, 591, 1064
 Bontemps, S., et al. 2001, *A&A*, 372, 173
 Boogert, A. C. A., Hogerheijde, M. R., Ceccarelli, C., Tielens, A. G. G. M., van Dishoeck, E. F., Blake, G. A., Latter, W. B., & Motte, F. 2002, *ApJ*, 570, 708
 Bouvier, J., & Appenzeller, I. 1992, *A&AS*, 92, 481
 Chelli, A., Cruz-Gonzalez, I., Zinnecker, H., Carrasco, L., & Perrier, C. 1988, *A&A*, 207, 46
 Chiang, E. I., & Goldreich, P. 1997, *ApJ*, 490, 368
 Cohen, J. G., Frogel, J. A., Persson, S. E., & Elias, J. H. 1981, *ApJ*, 249, 481
 Comeron, F., Rieke, G. H., Burrows, A., & Rieke, M. 1993, *ApJ*, 416, 185
 Dent, W. R. F., Matthews, H. E., & Walther, D. M. 1995, *MNRAS*, 277, 193
 Dolidze, M. V., & Arakelyan, M. A. 1959, *AZh*, 36, 444
 Doppmann, G., Jaffe, D., & White, R. J. 2003, *AJ*, 126, 3043
 Eisner, J. A., Lane, B. F., Akeson, R. L., Hillenbrand, L. A., & Sargent, A. I. 2003, *ApJ*, 588, 360
 Elias, J. 1978, *ApJ*, 224, 453
 Greene, T. P., & Lada, C. J. 1997, *AJ*, 114, 2157
 ———. 2002, *AJ*, 124, 2185
 Greene, T. P., & Meyer, M. R. 1995, *ApJ*, 450, 233
 Greene, T. P., Wilking, B. A., André, Ph., Young, E. T., & Lada, C. J. 1994, *ApJ*, 434, 614
 Greene, T. P., & Young, E. T. 1992, *ApJ*, 395, 516
 Haisch, K. E., Jr., Barsony, M., Greene, T. P., & Ressler, M. E. 2002, *AJ*, 124, 2841
 Haisch, K. E., Jr., Greene, T. P., Barsony, M., & Stahler, S. W. 2004, *AJ*, 127, 1747
 Haisch, K. E., Jr., Lada, E. A., & Lada, C. J. 2001, *ApJ*, 553, L153
 Jones, B., & Puetter, R. 1993, *Proc. SPIE*, 1946, 610
 Kamazaki, T., Saito, M., Hirano, N., Umemoto, T., & Kawabe, R. 2003, *ApJ*, 584, 357
 Kikuchi, N., Nakamoto, T., & Ogoshi, K. 2002, *PASJ*, 54, 589
 Lada, C. J. 1987, in *IAU Symp.* 115, *Star Forming Regions*, ed. M. Peimbert & J. Jugaku (Dordrecht: Reidel), 1
 Lada, C. J., & Wilking, B. A. 1984, *ApJ*, 287, 610
 Leous, J. A., Feigelson, E. D., André, Ph., & Montmerle, T. 1991, *ApJ*, 379, 683
 Looney, L. W., Mundy, L. G., & Welch, W. J. 2000, *ApJ*, 529, 477
 Luhman, K. L., & Rieke, G. H. 1999, *ApJ*, 525, 440
 Millan-Gabet, R., Schloerb, F. P., & Traub, W. A. 2001, *ApJ*, 546, 358
 Millan-Gabet, R., Schloerb, F. P., Traub, W. A., Malbet, F., Berger, J. P., & Bregman, J. D. 1999, *ApJ*, 513, L131
 Prato, L., Greene, T. P., & Simon, M. 2003, *ApJ*, 584, 853
 Ressler, M. E., & Barsony, M. 2001, *AJ*, 121, 1098
 ———. 2003, *ApJ*, 584, 832
 Ressler, M. E., Werner, M. W., Van Clever, J., & Chou, H. A. 1994, *Exp. Astron.*, 3, 277
 Rydgren, A. E., Strom, S. E., & Strom, K. M. 1976, *ApJS*, 30, 307
 Skrutskie, M., Dutkevitch, D., Strom, S., Edwards, S., & Strom, K. 1990, *AJ*, 99, 1187
 Strom, K. M., Kepner, J., & Strom, S. E. 1995, *ApJ*, 438, 813
 Strom, K. M., Strom, S. E., Edwards, S., Cabrit, S., & Skrutskie, M. F. 1989, *AJ*, 97, 1451
 Struve, O., & Rudkjøbing, M. 1949, *ApJ*, 109, 92
 Vrba, F. J., Strom, K. M., Strom, S. E., & Grasdalen, G. L. 1975, *ApJ*, 197, 77
 Walter, F. M., Vrba, F. J., Mathieu, R. D., Brown, A., & Myers, P. C. 1994, *AJ*, 107, 692
 Whitney, B. A., Wood, K., Bjorkman, J. E., & Cohen, M. 2003, *ApJ*, 598, 1079
 Wilking, B. A., Bontemps, S., Schuler, R. E., Greene, T. P., & André, Ph. 2001, *ApJ*, 551, 357
 Wilking, B. A., Greene, T. P., & Meyer, M. R. 1999, *AJ*, 117, 469
 Wilking, B. A., & Lada, C. J. 1983, *ApJ*, 274, 698
 Wilking, B. A., Lada, C. J., & Young, E. T. 1989, *ApJ*, 340, 823
 Young, E. T., Lada, C. J., & Wilking, B. A. 1986, *ApJ*, 304, L45